Cellular/Molecular

Separate Ca^{2+} Sources Are Buffered by Distinct Ca^{2+} Handling Systems in *Aplysia* Neuroendocrine Cells

Christopher J. Groten, Jonathan T. Rebane, Gunnar Blohm, and Neil S. Magoski

Department of Biomedical and Molecular Sciences, Graduate Program in Physiology, Centre for Neuroscience Studies, Queen's University, Kingston, Ontario K7L 3N6, Canada

Although the contribution of Ca^{2+} buffering systems can vary between neuronal types and cellular compartments, it is unknown whether distinct Ca^{2+} sources within a neuron have different buffers. As individual Ca^{2+} sources can have separate functions, we propose that each is handled by unique systems. Using *Aplysia californica* bag cell neurons, which initiate reproduction through an afterdischarge involving multiple Ca^{2+}-dependent processes, we investigated the role of endoplasmic reticulum (ER) and mitochondrial sequestration, as well as extrusion via the plasma membrane Ca^{2+}-ATPase (PMCA) and Na^+/Ca^{2+} exchanger, to the clearance of voltage-gated Ca^{2+} influx, Ca^{2+}-induced Ca^{2+}-release (CICR), and store-operated Ca^{2+} influx. Cultured bag cell neurons were filled with the Ca^{2+} indicator, fura-PE3, to image Ca^{2+} under whole-cell voltage clamp. A 5 Hz, 1 min train of depolarizing voltage steps elicited voltage-gated Ca^{2+} influx followed by EGTA-sensitive CICR from the mitochondria. A compartment model of Ca^{2+} indicated the effect of EGTA on CICR was due to buffering of released mitochondrial Ca^{2+} rather than uptake competition. Removal of voltage-gated Ca^{2+} influx was dominated by the mitochondria and PMCA, with no contribution from the Na^+/Ca^{2+} exchanger or sarcoplasmic/endoplasmic Ca^{2+}-ATPase (SERCA). In contrast, CICR recovery was slowed by eliminating the Na^+/Ca^{2+} exchanger and PMCA. Last, store-operated influx, evoked by ER depletion, was removed by the SERCA and depended on the mitochondrial membrane potential. Our results demonstrate that distinct buffering systems are dedicated to particular Ca^{2+} sources. In general, this may represent a means to differentially regulate Ca^{2+}-dependent processes, and for *Aplysia*, influence how reproductive behavior is triggered.

Introduction

Intracellular Ca^{2+} transduces electrical signals into biochemical cascades that control vital processes, including gene expression, excitability, and secretion (Clapham, 1995). Free Ca^{2+} is determined by the equilibrium between Ca^{2+} sources and Ca^{2+} removal (Catterall and Few, 2008). In neurons, Ca^{2+} enters primarily through voltage-gated Ca^{2+} channels, although the endoplasmic reticulum (ER) and mitochondria provide additional Ca^{2+} reservoirs for release (Armstrong and Hille, 1998; Rizzuto and Pozzan, 2006). Ca^{2+} removal relies on plasma membrane extrusion, controlled by the Na^+/Ca^{2+} exchanger and plasma membrane Ca^{2+}-ATPase (PMCA), and sequestration, mediated by the mitochondrial uniporter and sarcoplasmic/endoplasmic reticulum Ca^{2+}-ATPase (SERCA) (Kim et al., 2003, 2005; Rizzuto and Pozzan, 2006). The goal of this study is to examine the contribution of extrusion and sequestration to handling Ca^{2+} from different sources.

It is well established that the involvement of a given Ca^{2+} buffering system to the removal of a Ca^{2+} load varies between neuronal types and cytological compartments (Thayer and Miller, 1990; Fierro et al., 1998; Krizaj and Copenhagen, 1998; Morgans et al., 1998; Juhaszova et al., 2000; Holthoff et al., 2002; Kim et al., 2003, 2005). As the Ca^{2+}-dependent activation of downstream targets relies on a specific concentration and/or pattern of Ca^{2+}, this disparity likely reflects the different Ca^{2+} requirements for particular processes in a given neuron (e.g., motor vs sensory neuron) or compartment (e.g., dendrites vs axon terminal) (Caride et al., 2001; Berridge et al., 2003). Similar to different compartments, discrete Ca^{2+} sources can have unique roles in controlling neuronal function (Deisseroth et al., 1998; Berridge et al., 2000). Despite this, the relative contribution of given removal systems to the clearance of Ca^{2+} from distinct sources remains largely unexplored.

To address whether Ca^{2+} sources are handled uniquely, we used the bag cell neurons of the marine mollusk *Aplysia californica.* On stimulation, these neurons undergo ~30 min of action potential firing, known as an afterdischarge, during which egg-laying hormone (ELH) is secreted into the blood stream to initiate reproduction (Kupfermann and Kandel, 1970; Arch, 1972; Pinsker and Dudek, 1977). As the afterdischarge progresses, voltage-gated Ca^{2+} influx, Ca^{2+}-induced Ca^{2+}-release (CICR), and store-operated Ca^{2+} influx are engaged to provide the Ca^{2+} that orchestrates a sustained increase in excitability and neuropeptide secretion through various Ca^{2+}-dependent mechanisms (DeRiemer et al., 1984; Loechner et al., 1990; Wilson et al., 1996;

Received Dec. 20, 2011; revised Feb. 20, 2013; accepted Feb. 26, 2013.

Author contributions: C.J.G., J.T.R., G.B., and N.S.M. designed research; C.J.G. and J.T.R. performed research; C.J.G., J.T.R., and N.S.M. analyzed data; C.J.G. and N.S.M. wrote the paper.

This work was supported by Canadian Institutes of Health Research (CIHR) and Natural Sciences and Engineering Research Council of Canada (NSERC) operating grants to N.S.M. We thank H. M. Hodgson and S. L. Smith for technical assistance. C.J.G. holds a NSERC Post-Graduate Scholarship, and N.S.M. holds a CIHR New Investigator Award.

Correspondence should be addressed to Dr. Neil S. Magoski, Queen's University, Department of Biomedical and Molecular Sciences, 4th Floor, Botterell Hall, 18 Stuart Street, Kingston, ON K7L 3N6, Canada. E-mail: magoski@queensu.ca.

DOI:10.1523/JNEUROSCI.6384-11.2013

 0270-6474/13/336476-16$15.00/0

Michel and Wayne, 2002; Kachoei et al., 2006; Hung and Magoski, 2007). We show that voltage-gated Ca^{2+} influx is primarily sequestered by the mitochondria, which subsequently releases the Ca^{2+} to ultimately be extruded across the plasma membrane. A second plasma membrane Ca^{2+} source, store-operated Ca^{2+} influx, is preferentially cleared by the SERCA. Recent evidence from cervical ganglion neurons indicates that the differential contribution of removal systems can control which Ca^{2+} source activates a given intracellular pathway (Wheeler et al., 2012). By analogy, the differential Ca^{2+} clearance we observe in bag cell neurons may facilitate the production of source-specific Ca^{2+} profiles. This could ensure coupling to specific Ca^{2+} signaling pathways in the presence of multiple, spatiotemporally overlapping Ca^{2+} signals.

Materials and Methods

Animals and cell culture

Adult *Aplysia californica* (a hermaphrodite) weighing 150–500 g were obtained from Marinus. Animals were housed in an ~300 L aquarium containing continuously circulating, aerated artificial sea water (Instant Ocean, Aquarium Systems) at 14–16°C on a 12/12 h light/dark cycle and fed Romaine lettuce 5 times/week. For primary cultures of isolated bag cell neurons, animals were anesthetized by an injection of isotonic $MgCl_2$ (~50% body weight), the abdominal ganglion removed and incubated for 18 h at 22°C in neutral protease (13.33 mg/ml; 165859, Roche Diagnostics) dissolved in tissue culture artificial sea water (tcASW) (composition in mM: 460 NaCl, 10.4 KCl, 11 $CaCl_2$, 55 $MgCl_2$, 15 HEPES, 1 mg/ml glucose, 100 U/ml penicillin, and 0.1 mg/ml streptomycin, pH 7.8 with NaOH). The ganglion was then transferred to fresh tcASW and the bag cell neuron clusters were dissected from the surrounding connective tissue. Using a fire-polished Pasteur pipette and gentle trituration, neurons were dispersed onto 35 × 10 mm polystyrene tissue culture dishes (catalog #353001; Falcon, Becton Dickinson) filled with 2 ml of tcASW. Cultures were maintained in tcASW for 1–3 d in a 14°C incubator. Experiments were performed on neurons that were *in vitro* for at least 1 d. Salts were obtained from Fisher Scientific or Sigma-Aldrich.

Whole-cell, voltage-clamp recordings

Voltage-clamp recordings were made using an EPC-8 amplifier (HEKA Electronics) and the tight-seal, whole-cell method. Microelectrodes were pulled from 1.5 mm external, 1.2 mm internal diameter borosilicate glass capillaries (TW150F-4, World Precision Instruments) and had a resistance of 1–2.5 MΩ when filled with intracellular saline (see below). Pipette junction potentials were nulled, and subsequent to seal formation, pipette capacitive currents were cancelled. Following break-through, neuronal capacitance was also cancelled, and the series resistance (3–5 MΩ) compensated to 80% and monitored throughout the experiment. Current was filtered at 1 kHz with the EPC-8 Bessel filter and sampled at 2 kHz using a Digidata 1322A analog-to-digital converter (Molecular Devices), computer, and Clampex software (version 10.2, Molecular Devices). Voltage stimuli were delivered with Clampex.

Ca^{2+} currents were isolated using Ca^{2+}-Cs^+-tetraethylammonium (TEA) ASW, where the NaCl and KCl were replaced by TEA-Cl and CsCl, respectively, and the glucose and antibiotics were omitted (composition in mM: 460 TEA-Cl, 10.4 CsCl, 55 $MgCl_2$, 11 $CaCl_2$, 15 HEPES, pH 7.8 with CsOH). In some cases, the NaCl was not replaced by TEA to allow for Na^+/Ca^{2+} exchanger activity. Whole-cell recordings used a Cs^+-aspartate-based intracellular saline (composition in mM): 70 CsCl, 10 HEPES, 11 glucose, 10 glutathione, 5 ethyleneglycol bis (aminoethylether) tetraacetic acid (EGTA), 500 aspartic acid, 5 ATP (grade 2, disodium salt; A3377, Sigma-Aldrich), and 0.1 GTP (type 3, disodium salt; G8877, Sigma-Aldrich), pH 7.3 with CsOH. Certain experiments were performed with 0 mM EGTA in the internal saline. The majority of Ca^{2+}-imaging (see below) was performed under whole-cell voltage clamp, during which the intracellular saline was supplemented with 1 mM fura-PE3 (0110; Teflabs) (Vorndran et al., 1995) to dye-fill neurons via passive dialysis. Cells were dialyzed for at least 20 min before experiments were performed.

Sharp-electrode current-clamp recording

For store-operated Ca^{2+} influx, current clamp was used to inject fura-PE3 into bag cell neurons using a PMI-100 pressure microinjector (Dagan). Neurons were filled with an optimal concentration of dye, similar to whole-cell conditions. Microelectrodes were pulled from 1.2 mm external, 0.9 mm internal diameter borosilicate glass capillaries (IB120F-4; World Precision Instruments) and had a resistance of 15–30 MΩ when the tip was filled with 10 mM fura-PE3 and backfilled with 3 M KCl. Recordings were made using an Axoclamp 2B amplifier (Molecular Devices) and the sharp-electrode, bridge-balanced method. All neurons used for imaging had resting potentials of −50 to −60 mV and action potentials that overshot 0 mV after depolarizing current injection (0.5–1 nA, from the amplifier). Store-operated influx recordings were performed in Ca^{2+}-free ASW (composition as per tcASW but with added 0.5 mM EGTA and the glucose and antibiotics omitted) or Ca^{2+}/Na^+-free ASW [composition as per Ca^{2+}-free ASW but with Na^+ replaced with *N*-methyl-D-glucamine (NMDG)].

Ca^{2+} imaging

Imaging was performed using a TS100-F inverted microscope (Nikon) equipped with a Nikon Plan Fluor 10× [numerical aperture (NA) = 0.5], 20× (NA = 0.5), or 40× (NA = 0.6) objective. The light source was a 75 W Xenon arc lamp and a multiwavelength DeltaRAM V monochromatic illuminator (Photon Technology International) coupled to the microscope with a UV-grade liquid-light guide. Excitation wavelengths were 340 and 380 nm. Between acquisition episodes, the excitation illumination was blocked by a shutter, which along with the excitation wavelength, was controlled by a computer, a Photon Technology International computer interface, and EasyRatio Pro software (version 1.10, Photon Technology International). If image acquisition occurred at a frequency >0.2 Hz, the shutter remained open continuously. Emitted light passed through a 400 nm long-pass dichroic mirror and a 510/40 nm emission barrier filter before being detected by a Photometrics Cool SNAP HQ^2 charge-coupled device camera. Camera gain was maximized and exposure time adjusted on a per cell basis. Exposure times during 340 and 380 excitation were fixed to the same value. Background was removed by setting a minimal threshold value of 300 arbitrary units of fluorescence. Fluorescence intensities were typically sampled at 0.5 Hz. For longer recordings, sampling was switched to 0.2 Hz, after any fast periods of Ca^{2+} dynamics. Fluorescence signals were acquired using regions of interest measured over neuronal somata, at approximately the midpoint of the vertical focal plane and one-half to three-quarters of the cell diameter, then averaged eight frames per acquisition. The ratio of the emission following 340 and 380 nm excitation (340/380) was taken to reflect free intracellular Ca^{2+} (Grynkiewicz et al., 1985), and saved for subsequent analysis. Image acquisition, emitted light sampling, and ratio calculations were performed using EasyRatio Pro.

Reagents and drug application

Solution exchanges were accomplished by manual perfusion using a calibrated transfer pipette to first exchange the bath (tissue culture dish) solution. In most cases where a drug was applied, a small volume (≤10 μl) of concentrated stock solution was mixed with a larger volume of saline (~100 μl) that was initially removed from the bath, and this mixture was then pipetted back into the bath. Carbonyl cyanide 4-(trifluoromethoxy)phenylhydrazone (FCCP; 21857; Sigma-Aldrich), carboxyeosin (C-22803; Invitrogen), bafilomycin A (B1793, Sigma-Aldrich), and cyclopiazonic acid (CPA; C1530, Sigma-Aldrich or 239805, Calbiochem) all required dimethyl sulfoxide (DMSO; BP231, Fisher) as a vehicle. The maximal final concentration of DMSO was ≤0.5% (v/v) which, in control experiments as well as prior work from our laboratory, had no effect on membrane potential, various macroscopic or single-channel currents, resting intracellular Ca^{2+}, or Ca^{2+} transients evoked by a train of action potentials (Kachoei et al., 2006; Lupinsky and Magoski, 2006; Hung and Magoski, 2007; Gardam et al., 2008; Geiger and Magoski, 2008; Tam et al., 2009, 2011; Hickey et al., 2010). Tetraphenylphosphonium chloride (TPP; 218790, Sigma-Aldrich) and lanthanum chloride (La^{3+}; L-4131, Sigma-Aldrich) were prepared in water.

Analysis

Origin (version 7; OriginLab) was used to import and plot ImageMaster Pro files as line graphs. Analysis usually compared the steady-state value of the baseline 340/380 ratio with the ratio from regions that had reached a peak or new steady state. Averages of the baseline and peak regions were determined by eye or with adjacent-averaging. The rate of recovery of Ca^{2+} influx, after a stimulus train or store-operated Ca^{2+} entry and CICR, was quantified in different ways. To allow for comparison of data between our previous work on CICR (Geiger and Magoski, 2008), the rate of recovery from CICR was measured as the time required, after peak CICR, for the 340/380 ratio to return to 75% of the baseline ratio observed before the stimulus. The time at which the Ca^{2+} plateau first reached peak was considered time 0. Under circumstances where CICR was eliminated, time to 75% recovery was measured from the Ca^{2+} level at 1 min stimulation. This time was chosen because it reflects the typical point at which CICR responses peaked. Poststimulus area was used to quantify the magnitude and duration of CICR. Area was determined by integrating the region above the prestimulus baseline value from either 1 min post-train stimulus to 11 min or 11–21 min poststimulus. Again, measurements began at 1 min poststimulus to avoid including the initial recovery and capture peak CICR.

The degree of Ca^{2+} removal was also quantified by acquiring decay time constants and measuring the percentage recovery at 5 min poststimulus. Monoexponential decay functions were fit from the first point of decay to several minutes after complete recovery to baseline. The percentage recovery at 5 min was calculated by determining the degree of Ca^{2+} removed after the train stimulus or store-operated Ca^{2+} influx (340/380 peak–340/380 at 5 min post-peak) and dividing it by the peak rise during the response (340/380 peak–prestimulus baseline 340/380).

Summary data are presented as the mean ± SE). Statistics were performed using Instat (version 3.0; GraphPad Software). The Kolmogorov–Smirnov method was used to test datasets for normality. If the data were normal, Student's paired or unpaired *t* test (with the Welch correction as required) was used to test for differences between two means, whereas a standard one-way ANOVA with Dunnett's *post hoc* test was used to test for differences between multiple means. If the data were not normally distributed, a Mann–Whitney *U* test was used for two means, whereas a Kruskal–Wallis ANOVA with Dunn's *post hoc* test was used for multiple means. Fisher's exact test was used to test for differences in frequency between groups. A difference was considered significant if the two-tailed *p* value was <0.05.

For Figure 2, the rate of Ca^{2+} removal was determined for the post-train stimulus recovery period by deriving the slope of the Ca^{2+} decay ($[\Delta 340/380]/\Delta t$) at sequential time points using Microsoft Office Excel Plus 2010 (version 14). To prevent noise from influencing rate calculations, a fitted slope was measured starting at the initial decay point over 10 sequential time points ($[Ca]_n - [Ca]_{n+9}/t_n - t_{n+9}$) while incrementally shifting the start time ($n+1$) until the end of the decay phase. From this, a plot of Ca^{2+} decay rate versus 340/380 ratio was produced and fit with a second order polynomial function in Excel. Only traces that provided fits with $r^2 > 0.9$ were used for further analysis. Multiple polynomial fits were used to make an average polynomial function describing the dataset.

Model development

Equations describing mitochondrial Ca^{2+} dynamics were adapted from Colegrove et al. (2000b) to produce a compartment model of bag cell neuron Ca^{2+}.

Plasma membrane Ca^{2+} flux.

$$J_{influx} = k_{influx}([Ca^{2+}]_i - [Ca^{2+}]_e) \quad (1)$$

$$J_{efflux} = V_{max,efflux}/[1 + (EC_{50,efflux}/[Ca^{2+}]_i)^{n,efflux}] \quad (2)$$

$$J_{pm} = J_{influx} + J_{efflux}, \quad (3)$$

where J_{influx} is the rate of Ca^{2+} influx across the plasma membrane, k_{influx} refers to the Ca^{2+} permeability of the membrane, and $[Ca^{2+}]_i$ and $[Ca^{2+}]_e$ are the intracellular and extracellular Ca^{2+} concentrations, respectively. To produce Ca^{2+} influx in the model, k_{influx} was transiently increased and then reduced manually. J_{efflux} is the rate of plasma membrane efflux, $V_{max,efflux}$ is the maximal rate of efflux, $EC_{50,efflux}$ is the Ca^{2+} concentration at which efflux is half-maximal, and n_{efflux} is the Hill coefficient. J_{pm} is the net plasma membrane Ca^{2+} flux.

Mitochondrial Ca^{2+} dynamics.

$$J_{uptake} = k_{max,uptake}[Ca^{2+}]_i/[1 + (EC_{50,uptake}/[Ca^{2+}]_i)^{n,uptake}] \quad (4)$$

$$\delta([Ca^{2+}]_i) = 1.0 - 1.0/[1 + (K_{inhib}/[Ca^{2+}]_i)^{n,inhib}] \quad (5)$$

$$J_{release} = -\delta([Ca^{2+}]_i)V_{max,release}/(1 + EC_{50,release}/[Ca^{2+}]_m) \quad (6)$$

$$J_{mito} = J_{uptake} + J_{release}, \quad (7)$$

where J_{uptake} is the rate of mitochondrial Ca^{2+} sequestration, $k_{max,uptake}$ is the mitochondrial uptake rate constant, $EC_{50,uptake}$ describes the Ca^{2+} concentration at which uptake is half-maximal, and n_{uptake} is the Hill coefficient. The factor, $\delta([Ca^{2+}]_i)$, describes the inhibition of mitochondrial extrusion by cytosolic Ca^{2+}. K_{inhib} is the Ca^{2+} concentration at which inhibition of $J_{release}$ is half-maximal and n_{inhib} describes the sensitivity of inhibition to cytosolic Ca^{2+}. $V_{max,release}$ is the maximal rate of Ca^{2+} release from the mitochondria and $EC_{50,release}$ is the concentration of mitochondrial Ca^{2+} ($[Ca^{2+}]_m$) at which efflux rate is half of $V_{max,release}$. J_{mito} is the net Ca^{2+} flux of the mitochondria.

Exogenous Ca^{2+} buffers.

$$J_{EGTA} = (k_{off}[CaB] - k_{on}[Ca^{2+}]_i[B]), \quad (8)$$

where J_{EGTA} is the rate of free cytosolic Ca^{2+} removal by EGTA (Nowycky and Pinter, 1993), k_{off} and k_{on} are the reverse and forward reaction constants, respectively, $[CaB]$ is the concentration of the Ca^{2+}-EGTA complex, $[Ca^{2+}]_i$ is the concentration of cytosolic Ca^{2+}, and $[B]$ is the concentration of free EGTA. Values for k_{off} and k_{on} (Table 1) were taken from Naraghi (1997), whereas $[CaB]$ and $[B]$ were calculated from the total EGTA concentration using MaxChelator (http://maxchelator.stanford.edu/CaEGTA-NIST.htm).

Ca^{2+}-binding ratio.

$$\kappa = [B_t]K_d/([Ca^{2+}]_{i,rest} + K_d)([Ca^{2+}]_{i,peak} + K_d). \quad (9)$$

The variable, κ, represents the mean Ca^{2+}-binding ratio over the Ca^{2+} range experienced during typical neuronal excitation (Neher and Augustine, 1992). $[B_t]$ is the total buffer concentration, and K_d is the dissociation constant of the exogenous buffer. $[Ca^{2+}]_{i,rest}$ and $[Ca^{2+}]_{i,peak}$ are the free intracellular Ca^{2+} concentrations in the bag cell neurons at rest and during peak stimulus-induced influx, respectively.

Total Ca^{2+} removal rate.

$$d[Ca^{2+}]_T/dt = (d[Ca^{2+}]_F/dt)(1 + \kappa_s + \kappa_B). \quad (10)$$

For model presentation, rates of change in free intracellular Ca^{2+} ($d[Ca^{2+}]_F/dt$) were converted to rates of total Ca^{2+} removal ($d[Ca^{2+}]_T/dt$). κ_B represents the average Ca^{2+}-binding ratio for exogenous buffers (fura and EGTA) as calculated from Equation 9. Endogenous Ca^{2+}-binding ratios (κ_S) were taken from estimates in *Aplysia* metacerebral neurons (Gabso et al., 1997).

Collective Ca^{2+} dynamics.

$$d[Ca^{2+}]_i/dt = -(J_{pm} + J_{mito} + J_{EGTA}) \quad (11)$$

$$d[Ca^{2+}]_m/dt = J_{mito}/\gamma, \quad (12)$$

where $d[Ca^{2+}]_i/dt$ is the rate of change in cytosolic Ca^{2+}, $d[Ca^{2+}]_m/dt$ is the rate of change of mitochondrial Ca^{2+}, and γ is the ratio of effective mitochondrial and cytoplasmic volumes. The γ value used was taken from estimates in bullfrog sympathetic neurons (Colegrove et al., 2000b). For the estimates of model parameters, 340/380 ratios were converted to values of free intracellular Ca^{2+} based on Ca^{2+}-sensitive electrode recordings and fura K_d measurements in *Aplysia* (Fisher et al., 1994; Gabso

Table 1. Parameter values used in compartment model of bag cell neuron Ca^{2+}

Definition	Model variable	Standard value
Rate constant for PM Ca^{2+} influx	k_{influx}	5×10^{-6} (s^{-1})
Extracellular Ca^{2+} concentration	$[Ca^{2+}]_e$	11 mM
$[Ca^{2+}]_i$ at half maximal rate of efflux	$EC_{50,\ efflux}$	378.8 nM
Hill coefficient for efflux	n_{efflux}	1.8
Maximal rate of efflux*	$V_{max,\ efflux}$	4.06 ± 0.34 nM/s ($n = 15$)
$[Ca^{2+}]_i$ at half-maximal rate of mitochondrial uptake	$EC_{50,\ uptake}$	10 μM
Hill coefficient for mitochondrial Ca^{2+} uptake	n_{uptake}	2
Rate constant for mitochondrial Ca^{2+} uptake*	$k_{max,\ uptake}$	10.3 ± 0.88 s^{-1} ($n = 15$)
$[Ca^{2+}]_m$ at half-maximal rate of release	$EC_{50,\ release}$	307 nM
Maximal rate of mitochondrial Ca^{2+} release*	$V_{max,\ release}$	13.7 ± 4.0 nM/s ($n = 15$)
mitochondrial to cytosolic effective volume ratio	γ	2
$[Ca^{2+}]_i$ at half-maximal release inhibition	$EC_{50,\ inhib}$	500 nM
Hill coefficient for release inhibition	n_{inhib}	6
Dissociation constant of EGTA	$K_{d,\ EGTA}$	180 nM
Forward rate constant of EGTA	k_{on}	2.7 ± 10^6 $M^{-1} \cdot s^{-1}$
Reverse rate constant of EGTA	k_{off}	0.5 s^{-1}
Dissociation constant of fura	K_d	760 nM
Endogenous Ca^{2+} binding ratio	κ_e	60

*Indicates a free parameter estimated through data fitting (value ± SEM). All other parameters from the literature as indicated in text.

et al., 1997; Michel and Wayne, 2002). To fit individual traces, the $V_{max,\ efflux}$, $k_{max,\ uptake}$, and $V_{max,\ release}$ were left as free variables, whereas the constants (EC_{50} values) describing the Ca^{2+} sensitivity of plasma membrane extrusion and mitochondrial Ca^{2+} release were set to parameters established in bullfrog sympathetic neurons (Colegrove et al., 2000a,b). The components describing mitochondrial Ca^{2+} uptake ($EC_{50,\ uptake}$ and n_{uptake}) were based on measurements in isolated mitochondria and used to determine $k_{max,uptake}$ (Gunter and Pfeiffer, 1990; Gunter and Gunter, 1994; Colegrove et al., 2000b). Free parameters were then optimized to fit individual experimental records. Perhaps because of the time required for Ca^{2+} diffusion from the plasma membrane to the bulk of the cytosolic mitochondria, we found that proper fitting of bag cell neuron CICR often required a delayed onset of mitochondrial Ca^{2+} uptake. To account for this, our model implemented a time delay between the initial Ca^{2+} influx and the onset of mitochondrial buffering. The parameter estimates obtained from fitting were then collected from multiple neurons and averaged to obtain the values presented in Table 1. These values are shown as free, not total, intracellular Ca^{2+} to allow for comparison between similar models. Differential equations were solved numerically using Euler's method written in MATLAB with a time-step of 70 ms to produce graphical outputs of total cytosolic and mitochondrial Ca^{2+} over time.

Results

Mimicking the fast phase of the afterdischarge evokes distinct Ca^{2+} dynamics in bag cell neurons

A brief input to the bag cell neurons initiates the afterdischarge: a prolonged period of action potential firing consisting of a fast phase of ~5 Hz for ~1 min, which progresses into a slow phase of ~1 Hz for ~30 min (Kaczmarek et al., 1982; Fisher et al., 1994). To examine Ca^{2+} dynamics in response to a fast phase-like stimulus, a 1 min, 5 Hz train of 75 ms depolarizing steps to 0 mV was applied to fura-PE3-loaded, cultured bag cell neurons from a holding potential of −80 mV under whole-cell voltage clamp. Unless stated otherwise, all neurons were recorded using a Cs^+-containing and TEA-containing external solution (to replace K^+ and Na^+, respectively) and a Cs^+-containing internal pipette solution (to replace intracellular K^+; see Materials and Methods for details).

Application of the train stimulus produced a large, transient rise in intracellular Ca^{2+} due to the activation of voltage-gated Ca^{2+} channels, followed by an exponential decline, with recovery to baseline in 5–10 min ($n = 8$) (Fig. 1*A*, left). This response was measured with our Cs^+-based intracellular saline containing 5 mM Ca^{2+} chelator, EGTA. As this buffer alters free intracellular Ca^{2+}, we sought to apply the same stimulus when EGTA was omitted from the pipette solution. With 0 mM intracellular EGTA, excitation again resulted in a large Ca^{2+} transient; however, a prolonged Ca^{2+} plateau, often marked by a delayed peak, now followed the initial recovery ($n = 6$) (Fig. 1*A*, right). This Ca^{2+} plateau long outlasted the duration of the stimulus, and was followed by a slow return to baseline within 10–20 min. Similar sequences of changes to intracellular Ca^{2+} have been described as CICR in dorsal root ganglion neurons, bullfrog sympathetic neurons, adrenal chromaffin cells, and *Aplysia* neuron R15 (Gorman and Thomas, 1980; Friel and Tsien, 1994; Herrington et al., 1996; Colegrove et al., 2000a).

Removing intracellular EGTA significantly reduced the peak percentage change in intracellular Ca^{2+} during the train stimulus compared with 5 mM EGTA (Fig. 1*B*, left). This is likely due to a facilitation of Ca^{2+}-dependent inactivation of voltage-gated Ca^{2+} channels and an increase in resting Ca^{2+} levels (5 mM EGTA resting 340/380: 0.18 ± 0.004, $n = 8$; 0 mM EGTA resting 340/380: 0.26 ± 0.01, $n = 6$; $p < 0.003$, unpaired Mann–Whitney *U* test). The area from 1 to 11 min poststimulus train (10 min total) was used to quantify the magnitude and duration of the Ca^{2+} plateau (see Materials and Methods for details). The presence of the Ca^{2+} plateau in 0 mM EGTA was reflected by a significant increase in poststimulus train area from 1 to 11 min (Fig. 1*B*, middle) and the time to 75% recovery from peak post-train stimulus Ca^{2+} (Fig. 1*B*, right). Thus, mimicking an endogenous firing pattern evoked distinct rapid and slow periods of cytosolic Ca^{2+} dynamics in the bag cell neurons. As the transduction of a Ca^{2+} signal to activate unique biochemical pathways relies on the temporal and spatial properties of intracellular Ca^{2+}, we sought to dissect the Ca^{2+} sources and removal processes that contributed to these Ca^{2+} responses.

Voltage-gated Ca^{2+} influx from a train stimulus is cleared by mitochondrial uptake

Mitochondria are an essential Ca^{2+} removal system in many neurons and neuroendocrine cells, particularly when Ca^{2+} concentrations are substantially higher than at rest (>500 nM) (Herrington et al., 1996). Prior work by our lab indicated a role for mitochondrial Ca^{2+} uptake after a train of action potentials (Geiger and Magoski, 2008). To test whether the mitochondria are

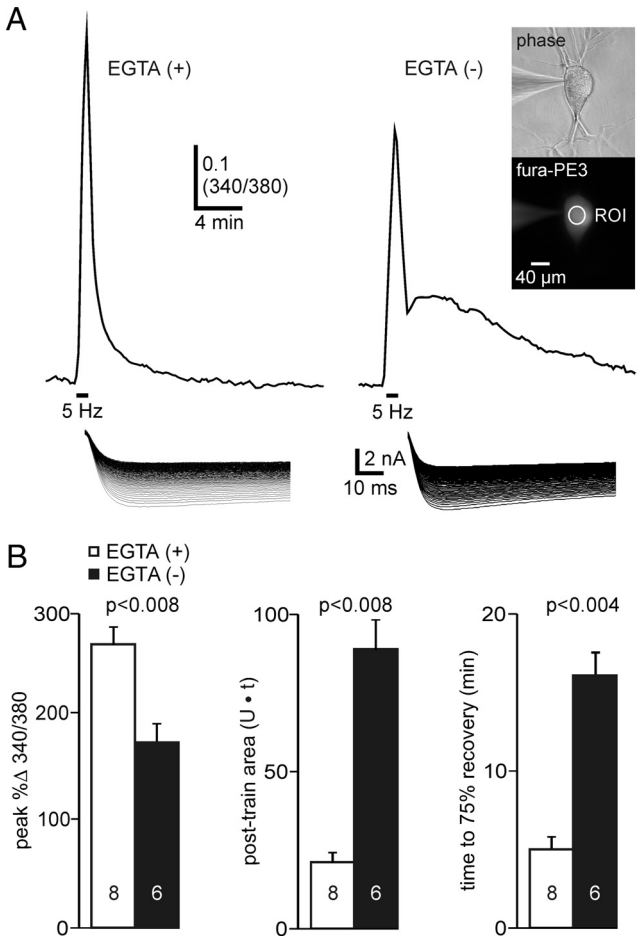

Figure 1. A train of depolarizing stimuli induces a secondary Ca^{2+} rise sensitive to the Ca^{2+} chelator, EGTA. ***A***, Simultaneous measurement of free intracellular Ca^{2+} and membrane current in cultured bag cell neurons using 340/380 fura PE3 fluorescence and whole-cell voltage clamp at −80 mV. ***A***, Inset, A phase contrast image shows the recording pipette, bag cell neuron soma, and its neuritic processes. The bottom image shows the same neuron loaded with fura and the somatic region of interest (ROI) used for data collection. Scale bar applies to both images. ***A***, Top left, Ca^{2+} influx indicated by a change in intensity of the 340/380 fluorescence ratio following a 1 min, 5 Hz train of 75 ms steps from −80 to 0 mV. With 5 mM intracellular EGTA, stimulation causes a large rise in Ca^{2+} followed by a rapid recovery to the prestimulus baseline. Top right, In the absence of intracellular EGTA, there is a prolonged Ca^{2+} plateau subsequent to the initial influx that greatly outlasts the stimulus duration, indicative of CICR. ***A***, Bottom, Traces depict 300 overlaid Ca^{2+} currents from each pulse to 0 mV of the 1 min train stimulus in either 5 or 0 mM intracellular EGTA. The shifting band of traces is due to use-dependent inactivation of Ca^{2+} currents during the train stimulus. Unless stated otherwise, all cells were recorded in a Cs^+-external and TEA-external (to replace K^+ and Na^+, respectively) and a Cs^+-based intracellular solution (to replace intracellular K^+). ***B***, Left, The percentage change in 340/380 from baseline to the peak response during the train stimulus is significantly larger in 5 mM EGTA versus 0 mM EGTA (unpaired Student's *t* test). For this and subsequent bar graphs, data represents the mean ± SE, and the *n*-value is indicated within the bars. ***B***, Middle and right, Zero mM EGTA significantly increases the total area measured from 1 min after stimulation to 11 min post-train stimulus (Mann–Whitney *U* test) and the time to reach 75% recovery to baseline Ca^{2+} from the peak of the plateau (Mann–Whitney *U* test).

key to removal of voltage-gated Ca^{2+} influx, the ability of mitochondria to clear Ca^{2+} was eliminated using FCCP. This protonophore collapses the mitochondrial membrane potential, releases stored Ca^{2+}, and prevents subsequent Ca^{2+} uptake into the organelle (Heytler and Prichard, 1962; Babcock et al., 1997). EGTA (5 mM) was included in the pipette solution to eliminate the Ca^{2+} plateau and allow for isolated measurement of voltage-gated Ca^{2+} influx and removal. Post-train stimulus recoveries were well fit with monoexponential decay functions, from which time constants were derived to quantify changes in Ca^{2+} clearance. Percentage recovery at 5 min was measured to quantitate the degree of Ca^{2+} recovery. Any sample size discrepancy between percentage recovery and decay constants for the same dataset was because of the exclusion of poor exponential fits.

Initial observations showed that some neurons treated with FCCP had a reduced peak rise in Ca^{2+} during the train stimulus. This may be because of an increase in use-dependent inactivation of Ca^{2+} currents in the absence of mitochondrial Ca^{2+} clearance. To prevent this from impacting quantification of Ca^{2+} removal, additional FCCP-treated neurons were stimulated with 5 Hz, 1 min train of 175 ms pulses to enhance Ca^{2+} influx and match the peak levels seen in controls. Cells that presented peak Ca^{2+} amplitudes comparable to control were used in measuring the percentage recovery. As such, peak Ca^{2+} influx was not significantly different between DMSO-treated and selected FCCP-treated neurons (DMSO peak % Δ 340/380: 135.4 ± 8.8, $n = 10$; FCCP peak % Δ 340/380: 162.3 ± 14.5, $n = 12$; $p > 0.05$, unpaired Student's *t* test).

Compared with DMSO-treated cells, neurons stimulated after a 30 min exposure to 20 μM FCCP presented a slower Ca^{2+} recovery (Fig. 2*A*), as indicated by a significantly larger decay time constant (Fig. 2*A*, inset). These findings are consistent with the effects of FCCP in other systems, and indicate a role for mitochondrial Ca^{2+} clearance (Thayer and Miller, 1990; Friel and Tsien, 1994; Werth and Thayer, 1994). From the decay of these Ca^{2+} transients, we determined the relative rate of apparent mitochondrial uptake (R_{mit}) by subtracting the rate of Ca^{2+} removal in FCCP conditions (R_{FCCP}) from the total Ca^{2+} removal rate (R_{total}) at corresponding 340/380 ratio values (see Materials and Methods for details). Figure 2*B* (top) displays the relative cytosolic Ca^{2+} removal rate, normalized to peak rate, against the 340/380 ratio for the representative traces in Figure 2*A*, along with fitted polynomial functions. Fits from multiple neurons were used to produce averaged R_{FCCP}, R_{total}, and R_{mit} values (Fig. 2*B*, bottom). This suggests that mitochondrial uptake occurred over a wide range of Ca^{2+} levels, both at rest and at peak values during stimulation, with a corresponding increase in removal rate. In contrast, the nonmitochondrial Ca^{2+} buffer, represented as R_{FCCP}, had a shallower slope over the same range, indicating the presence of a relatively slow removal mechanism.

Central to the notion that the mitochondria buffer voltage-gated Ca^{2+} influx, is that there is an increase in mitochondrial Ca^{2+} after stimulation. To examine this, FCCP was used to liberate mitochondrial Ca^{2+}, with or without a prior train stimulus. Assuming mitochondrial involvement, 100 μM tetraphenylphosphonium (TPP), a blocker of mitochondrial Ca^{2+} exchange in bag cell neurons (Karadjov et al., 1986; Geiger and Magoski, 2008), was applied to both DMSO-treated and FCCP-treated cells, to ensure no mitochondrial Ca^{2+} release followed the excitation. As per prior work suggesting the mitochondria of cultured bag cell neurons contain Ca^{2+} at rest (Jonas et al., 1997; Gardam et al., 2008; Geiger and Magoski, 2008), bath application of 20 μM FCCP increased cytosolic Ca^{2+} within 5 min ($n = 6$) (Fig. 2*C*, left). If a train stimulus was delivered before FCCP ($n = 6$), the Ca^{2+} release signal was significantly increased by ~40%, consistent with voltage-gated Ca^{2+} influx enhancing the amount of Ca^{2+} stored in the mitochondria (Fig. 2*C*, right, *D*).

As mitochondria appear to be essential for Ca^{2+} removal after depolarization, we attempted to saturate Ca^{2+} clearance with and without active mitochondria. After a 5 Hz, 1 min train stimulus in FCCP ($n = 5$), Ca^{2+} often decayed slowly to a higher level than the prestimulus baseline (Fig. 2*E*). Application of a second

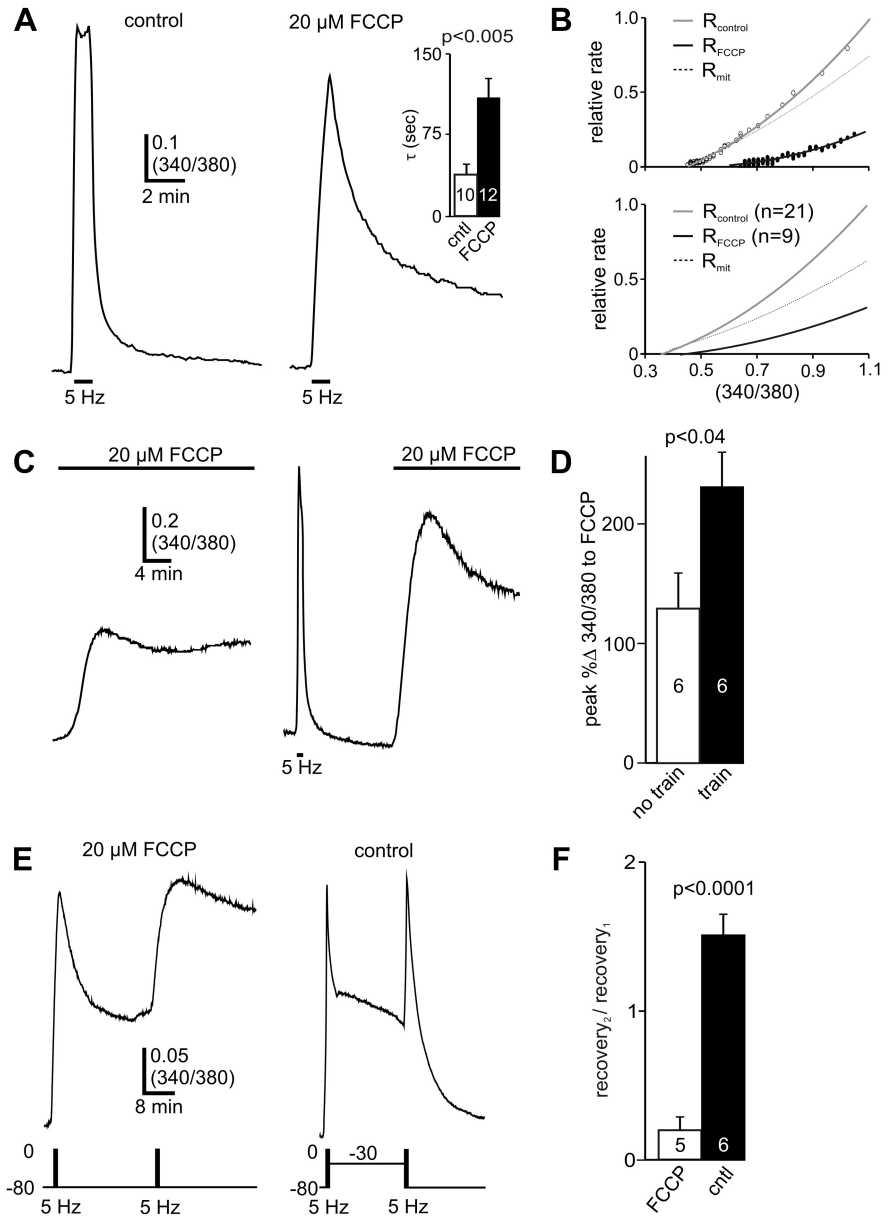

Figure 2. Mitochondria remove voltage-gated Ca^{2+} influx and clear Ca^{2+} from repeated stimuli. ***A***, Neurons voltage-clamped to −80 mV with 5 mM intracellular EGTA to allow for isolated measurement of voltage-gated Ca^{2+} influx and removal. ***A***, Left, In DMSO, cytosolic Ca^{2+} transients evoked by the 5 Hz, 1 min train stimulus are followed by rapid recovery to baseline Ca^{2+}. ***A***, Right, Pretreatment with 20 μM FCCP, a protonophore that collapses the mitochondrial membrane potential and prevents Ca^{2+} sequestration, slows the recovery of Ca^{2+} following stimulation. ***A***, Inset, The exponential decay time constant (τ) of the Ca^{2+} transient recovery phase is significantly larger in FCCP-treated neurons (unpaired Student's *t* test). ***B***, Top, Relative Ca^{2+} clearance rate (R), calculated from the decay phase of Ca^{2+} transients shown in ***A***, as a function of 340/380 ratio (rates normalized to the maximal value of the 340/380 range). Second-order polynomial fitted lines are plotted overtop of the data points. The difference between the control (R_{total}) and FCCP (R_{FCCP}) fits produce the estimated mitochondrial uptake (R_{mit}), represented by the light dashed line. ***B***, Bottom, Second-order polynomial fit lines for $R_{control}$, R_{FCCP}, and R_{mit} representing averaged removal rates from multiple neurons. Sample sizes are different from the decay time constants shown in ***A*** due to quality of fit criteria required for rate functions (see Materials and Methods). ***C***, Ca^{2+} influx from a train stimulus loads mitochondria with Ca^{2+}. ***C***, Left, FCCP (20 μM) elevates Ca^{2+} in neurons under voltage clamp at −80 mV with 5 mM EGTA in the pipette and 100 μM TPP to prevent potential release of mitochondrial Ca^{2+}. ***C***, Right, FCCP-induced Ca^{2+} release after a large influx of Ca^{2+} from a 5 Hz, 1 min train stimulus is increased. ***D***, Train stimulation, before FCCP application, significantly enhances the peak percentage change upon FCCP-induced Ca^{2+} liberation (unpaired Student's *t* test). ***E***, Mitochondrial Ca^{2+} clearance is necessary for recovery from repeated stimuli. ***E***, Left, After a train stimulus in FCCP, a second stimulus produces a Ca^{2+} load that is largely unremoved. ***E***, Right, To replicate the slow Ca^{2+} recovery in FCCP, a control cell is given a train stimulus, but then subsequently held at −30 mV to allow for a small persistent Ca^{2+} influx. Ca^{2+} levels are quickly restored following a second train stimulus when the cell is clamped at −80 mV. ***F***, The ratio between the first and second percentage recovery at 5 min is significantly larger in FCCP-treated neurons (unpaired Student's unpaired *t* test).

train stimulus from this new baseline elevated Ca^{2+} to similar levels as the first train stimulus; however, the subsequent recovery was severely hindered (Fig. 2*E*, left). To control for differences between FCCP and control in Ca^{2+} after the first train stimulus, DMSO-treated neurons were held at a potential ranging from −20 to −30 mV immediately after the first train stimulus ($n = 6$). Because some neurons had smaller Ca^{2+} currents, a range of voltages was used to ensure that all Ca^{2+} plateaus were of comparable size. Voltage-clamping at the depolarized potential produced an elevated Ca^{2+} baseline similar to that seen in FCCP. After the second train stimulus, cells were again held at −80 mV, but unlike in FCCP, DMSO-treated cells recovered rapidly to the Ca^{2+} levels as seen at the start of the experiment (Fig. 2*E*, right). The ratio between the percentage recovery at 5 min after the first and second train stimulus was used to quantify the degree of buffer saturation in each condition. The percentage recovery ratio was significantly reduced in FCCP-treated compared with DMSO-treated neurons (Fig. 2*F*).

Contribution of the plasma membrane Ca^{2+} ATPase to the removal of voltage-gated Ca^{2+} influx

Although our results strongly suggest that mitochondria are the predominant buffer for voltage-gated Ca^{2+} influx, a residual contribution from other systems must exist, given the slow recovery even in the presence of FCCP. Most cells use the high-affinity, low-capacity PMCA to extrude Ca^{2+} across the plasma membrane (Sanchez-Armass and Blaustein, 1987; Blaustein and Lederer, 1999; Jeon et al., 2003; Tidow et al., 2012). The role of this pump in removing voltage-gated Ca^{2+} influx was tested with 2 mM extracellular La^{3+}, a common PMCA inhibitor (Carafoli, 1991; Herrington et al., 1996; Zenisek and Matthews, 2000). Addition of La^{3+} ~1 s subsequent to the end of the 5 Hz, 1 min train stimulus ($n = 16$) slowed the recovery to prestimulus baseline (Fig. 3*A*, left) compared with control neurons treated with water ($n = 17$). This manifested as a significantly smaller percentage recovery at 5 min poststimulus in La^{3+}-treated neurons (Fig. 3*C*). Consistent with a minor role of the PMCA in removing Ca^{2+}, La^{3+} appeared to have a smaller effect on percentage recovery than FCCP (Fig. 3*C*). Because La^{3+} was bath applied on the last pulse of the train stimulus, to avoid blocking Ca^{2+} currents, the onset of La^{3+} action was delayed for several sec-

onds thereafter. Thus, post-train stimulus decay time constants were not determined for this experiment, as they would not have been an accurate reflection of PMCA inhibition.

The plasma membrane Na^+/Ca^{2+} exchanger trades extracellular Na^+ for intracellular Ca^{2+} (Blaustein and Lederer, 1999; Kim et al., 2003). In the bag cell neurons, Na^+/Ca^{2+} exchanger activity can be eliminated by replacing extracellular Na^+ with TEA (Knox et al., 1996). Our standard recording conditions used extracellular TEA, rather than Na^+; thus, we tested the effect of supplementing extracellular Na^+ in lieu of TEA on the rate of voltage-gated Ca^{2+} removal (Fig. 3*A*). Compared with TEA ($n = 6$), adding extracellular Na^+ ($n = 7$) did not significantly alter the magnitude of the Ca^{2+} rise during stimulation (TEA peak % Δ: 174.9 ± 18.8, $n = 6$; Na^+ peak % Δ: 150.5 ± 22.3, $n = 7$; $p > 0.05$, unpaired Student's *t* test), poststimulus Ca^{2+} decay time constant (Fig. 3*B*) or the percentage recovery at 5 min after peak Ca^{2+} (Fig. 3*C*).

In addition to the mitochondria, the ER is the other primary intracellular Ca^{2+} store in neurons (Berridge et al., 2000), and has been found to remove voltage-gated Ca^{2+} influx in neurons and neuroendocrine cells (Fierro et al., 1998; Kim et al., 2003). To test this in bag cell neurons, 20 μM CPA, a SERCA inhibitor found to be effective in bag cell neurons (Seidler et al., 1989; Kachoei et al., 2006; Gardam et al., 2008; Geiger and Magoski, 2008), was applied 30 min before stimulation. Post-train stimulus Ca^{2+} kinetics were not affected by the presence of CPA ($n = 6$) versus control ($n = 7$) (Fig. 3*A*). CPA did not alter the peak rise in Ca^{2+} during stimulation (DMSO peak % Δ: 174.3 ± 20.4, $n = 7$; CPA peak % Δ: 164.8 ± 26.2, $n = 6$; $p > 0.05$, unpaired Student's *t* test), the poststimulus Ca^{2+} decay time constant (Fig. 3*B*), or the percentage recovery to baseline following stimulation (Fig. 3*C*).

Finally, FCCP also collapses other stores with proton gradients, including lysosome, endosomes, and secretory vesicles (Goncalves et al., 1999; Christensen et al., 2002). The contribution of these stores to the removal of voltage-gated Ca^{2+} influx was tested by treating cells with bafilomycin A, a H^+-ATPase inhibitor that prevents the sequestration of Ca^{2+} by acidic stores (Bowman et al., 1988; Goncalves et al., 1999). Our earlier work demonstrated that bafilomycin A causes a slow, steady increase in bag cell neuron cytosolic Ca^{2+}, distinct from the response to other liberating agents (Kachoei et al., 2006; Hickey et al., 2010). Pretreatment with 100 nM bafilomycin A ($n = 6$) did not alter the post-train stimulus Ca^{2+} removal compared with DMSO-treated neurons ($n = 6$) (Fig. 3*A*). Bafilomycin did not change the post-stimulus decay time constant (Fig. 3*B*), the percentage recovery at 5 min after peak Ca^{2+} (Fig. 3*C*) or the peak Ca^{2+} rise (DMSO peak % Δ: 235.58 ± 18.3, $n = 6$; bafilomycin A peak % Δ: 233.0 ± 23.7, $n = 6$; $p > 0.05$, unpaired Student's *t* test). Thus, the effect of FCCP on Ca^{2+} removal was due its action on mitochondrial function.

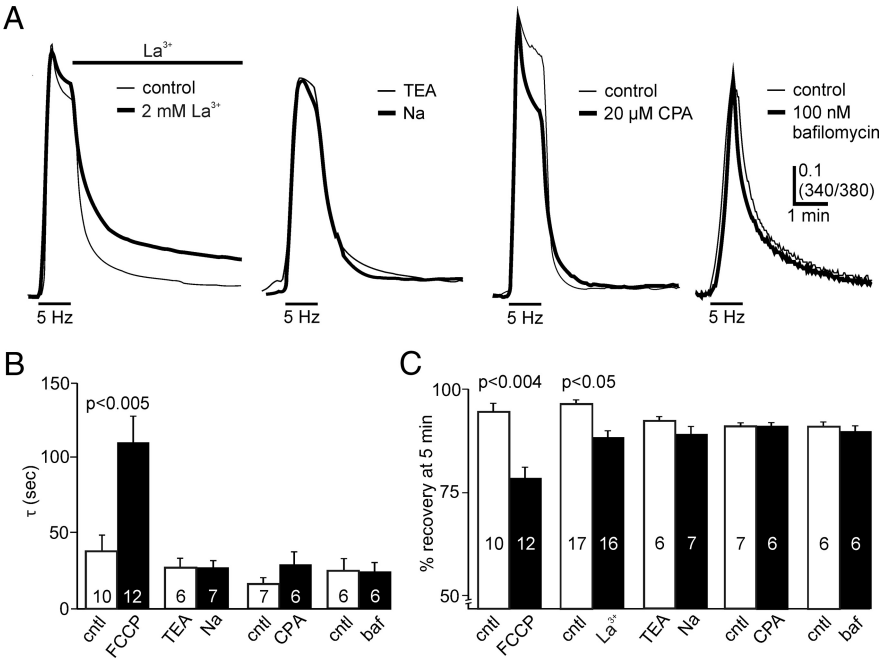

Figure 3. Removal of voltage-gated Ca^{2+} influx is slowed by inhibition of the PMCA, but is not influenced by acidic stores, ER, or the Na^+/Ca^{2+}-exchanger. ***A***, Left, Blocking PMCA function by the addition of 2 mM extracellular La^{3+} on the last pulse of the 1 min, 5 Hz train stimulus, hinders Ca^{2+} removal (dark trace), whereas H_2O (control) (light trace) applied in the same manner has no effect. ***A***, Middle left, In contrast, the inclusion of Na^+ (dark trace) rather than TEA (light trace) in the extracellular saline, to permit Na^+/Ca^{2+} exchanger activity, has no effect. Similarly, treatment with 20 μM CPA (middle right), to inhibit SERCA, or 100 nM bafilomycin A (baf) (right), to prevent uptake by acidic stores, does not alter Ca^{2+} removal after a train stimulus. ***B***, Neurons treated with 20 μM FCCP present significantly larger exponential decay time constants (τ) relative to controls (reproduced from Fig. 2*A*), whereas cells in the presence of extracellular Na^+, exposed to CPA, or baf do not have significantly different τ values (all comparisons using unpaired Student's *t* test). ***C***, FCCP (Mann–Whitney *U* test) and La^{3+} significantly (Welch corrected unpaired Student's *t* test) reduce the percentage recovery at 5 min post-train stimulus whereas extracellular Na^+, CPA, and baf have no effect (all comparisons using unpaired Student's *t* test).

The PMCA, but not the SERCA or Na^+/Ca^{2+} exchanger, clear somatic Ca^{2+} in the absence of mitochondrial function

The inhibition of a dominant Ca^{2+} clearance system can unveil the activity of other, formerly uninvolved removal mechanisms (Zenisek and Matthews, 2000; Kim et al., 2005). This presumably reflects a compensatory property that ensures normal Ca^{2+} homeostasis. We examined this possibility in bag cell neurons by exploring the contribution of nonmitochondrial clearance mechanisms in the presence of FCCP. Addition of the PMCA inhibitor, La^{3+}, to the extracellular solution on the last pulse of the 5 Hz, 1 min train stimulus ($n = 7$), significantly blunted the recovery from peak compared with FCCP alone ($n = 5$). In the presence of FCCP, once full PMCA inhibition manifested, little to no recovery occurred and Ca^{2+} remained at a much higher plateau than in FCCP alone (Fig. 4*A*, left). The percentage recovery at 5 min was significantly reduced under these conditions (Fig. 4*C*). These data indicates that in the absence of both mitochondrial and PMCA function, voltage-gated Ca^{2+} removal is largely occluded. In contrast, exchanging extracellular Na^+ ($n = 7$) for TEA ($n = 8$), or pretreatment with CPA (control, $n = 8$; CPA, $n = 8$) remained ineffective at influencing post-train stimulus Ca^{2+} removal in the absence of mitochondrial function (Fig. 4*A*, middle, right). Poststimulus decay time constants (Fig. 4*B*) and percentage recoveries at 5 min (Fig. 4*C*) were unchanged by including extracellular Na^+ or pretreatment with CPA.

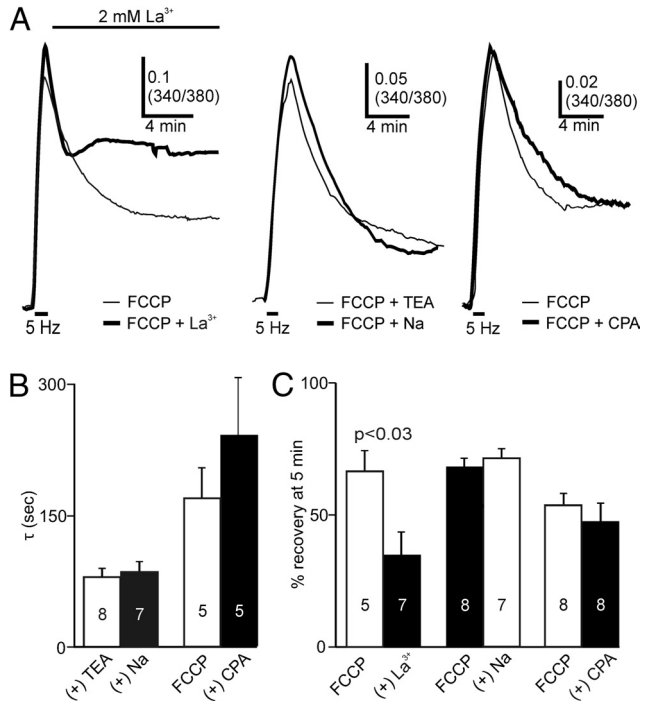

Figure 4. In the absence of mitochondrial function, PMCA, but neither SERCA nor the Na^+/Ca^{2+}-exchanger, influence the removal of voltage-gated Ca^{2+} influx. ***A***, Left, Post-stimulus addition of the PMCA inhibitor, La^{3+} (2 mM) (dark trace), in the presence of 20 μM FCCP, strongly attenuates the subsequent recovery relative to FCCP alone (light trace). The inclusion of extracellular Na^+ (middle) or pretreatment with 20 μM CPA (right) does not influence Ca^{2+} removal in the presence of FCCP. ***B***, For neurons pretreated with FCCP, the mean post-train stimulus recovery τ values are not significantly altered by the inclusion of extracellular Na^+ or exposure to CPA (unpaired Student's *t* test and Mann–Whitney *U* test, respectively). ***C***, Summary of mean percentage recovery at 5 min post-train stimulus. In the presence of FCCP, La^{3+} significantly increases the percentage recovery at 5 min, whereas the application CPA (Mann–Whitney *U* test) or the inclusion of extracellular Na^+ remains ineffective (all other comparisons using unpaired Student's *t* tests).

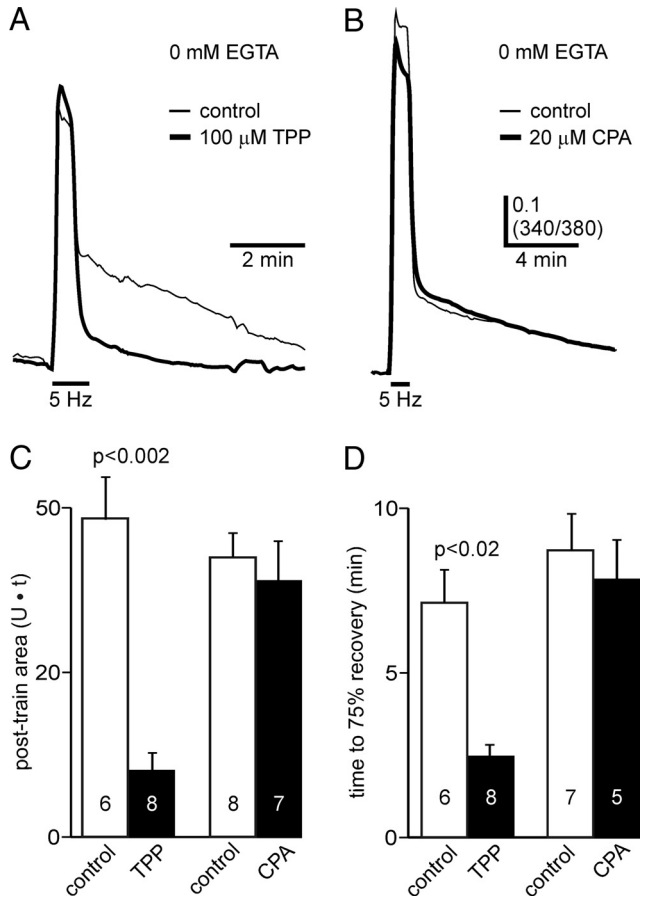

Figure 5. The EGTA-sensitive Ca^{2+} plateau is caused by mitochondrial Ca^{2+} release. ***A***, A post-stimulus Ca^{2+} plateau is evoked by a 5 Hz, 1 min train of depolarizing steps under voltage clamp. Intracellular EGTA is absent (0 mM) to allow for CICR. The prolonged Ca^{2+} plateau in control conditions (light trace) is substantially smaller in 100 μM the mitochondrial Ca^{2+} exchange blocker, TPP (dark trace). ***B***, Treatment with CPA, to inhibit SERCA and prevent ER Ca^{2+} release, does not affect the post-train stimulus Ca^{2+} plateau (dark trace) when compared with DMSO-treated neurons (light trace). ***C***, ***D***, TPP but not CPA, significantly reduces the 1–11 min area relative to controls (unpaired Student's *t* test in both cases). TPP also significantly reduces the time to reach 75% recovery of baseline Ca^{2+} from peak CICR (Welch corrected, unpaired Student's *t* test). In contrast, CPA has no significant effect on the recovery time (unpaired Student's *t* test). Sample sizes for the time to 75% recovery in CPA are smaller than those used for post-stimulus area measurements as some neurons did not achieve 75% recovery.

The EGTA-sensitive Ca^{2+} plateau is caused by mitochondrial Ca^{2+} release

In many neurons, it is common for brief periods of action potential firing to evoke sustained Ca^{2+} release from mitochondria or the ER with similar characteristics as the EGTA-sensitive Ca^{2+} plateau shown in Figure 1 (Gorman and Thomas, 1980; Smith et al., 1983; Neering and McBurney, 1984; Tang and Zucker, 1997; Lee et al., 2007). Prior research from our lab has found that prolonged stimulation of bag cell neurons under sharp electrode recording elicited a CICR plateau that was sensitive to FCCP as well as TPP, an inhibitor of mitochondrial Ca^{2+} exchangers (Geiger and Magoski, 2008). To determine whether the EGTA-sensitive Ca^{2+} plateau we observed under whole-cell conditions was also due to mitochondrial Ca^{2+} release, 100 μM TPP was applied to cells 30 min before stimulation. In the presence of TPP ($n = 8$), the post-train stimulus response transformed from a slow, large Ca^{2+} plateau under control conditions ($n = 6$) to a rapid exponential recovery indistinguishable from that seen in 5 mM intracellular EGTA (compare Figs. 5*A*, 1*A*). This was apparent from the significantly reduced post-train stimulus area from 1 to 11 min (Fig. 5*C*) and time to 75% recovery from peak Ca^{2+} (Fig. 5*D*). TPP had this effect without altering the peak rise in Ca^{2+} during stimulation (control peak % Δ: 127.5 ± 7.4, $n = 6$; TPP peak % Δ: 127.6 ± 11.5, $n = 8$; $p > 0.05$ unpaired Student's *t* test).

To determine whether CICR from the ER contributed to the plateau, CPA was used to deplete the ER of Ca^{2+} before stimulation. Cells treated with 20 μM CPA ($n = 7$) presented a similar Ca^{2+} plateau magnitude as in control conditions ($n = 8$) and recovered to prestimulus baseline with a comparable time course (Fig. 5*B*). CPA did not significantly alter post-train stimulus area from 1 to 11 min (Fig. 5*C*) and did not affect the time to 75% recovery from peak Ca^{2+} (Fig. 5*D*). These results indicate that the EGTA-sensitive Ca^{2+} plateau is mitochondrial, but not ER, Ca^{2+} release, and that removal of CICR is independent of the SERCA.

CICR is removed by plasma membrane extrusion via Na^+/Ca^{2+} exchange and the PMCA

As the Ca^{2+} plateau from mitochondrial release had a different magnitude and kinetics than voltage-gated Ca^{2+} influx during the train stimulus, it is possible that the handling mechanisms responsible for CICR are different from those for voltage-gated Ca^{2+}. Full recovery from CICR typically required >10 min; therefore, we presumed that a relatively slow clearance system was responsible for its removal. To examine this, we first tested for the contribution of the Na^+/Ca^{2+} exchanger by substituting

extracellular Na^+ for TEA. In contrast to its ineffectiveness in removing voltage-gated Ca^{2+} influx, extracellular Na^+ significantly reduced the time to 75% recovery from peak CICR to baseline (Fig. 6*A*, left) compared with TEA. However, the post-train stimulus area from 1 to 11 min was not significantly different between Na^+ and TEA conditions (Fig. 6*B*). This occurred because the first stage of CICR is marked by the rising Ca^{2+} plateau, which was not significantly different in magnitude between TEA and Na^+ conditions (TEA external, peak % Δ: 86.3 ± 2.0, $n = 7$; Na^+ external, peak % Δ: 79.6 ± 5.0, $n = 12$; $p > 0.05$, Mann–Whitney *U* test). Nevertheless, the area from 11 to 21 min post-train stimulus, where the recovery from peak is most prominent, was significantly smaller in the presence of extracellular Na^+ (Fig. 6*B*). Sample size between time to 75% recovery and post-train stimulus area for Na^+-conditions was different because one cell did not recover to 75% by the end of the recording.

Even in the presence of TEA, when the Na^+/Ca^{2+} exchanger was inhibited, CICR recovery still occurred, albeit at a slower rate, indicating involvement of another removal system. To determine whether the PMCA was responsible, 2 mM La^{3+} was applied at the peak of CICR, ~1 min post-train stimulus, while in the presence of extracellular TEA. PMCA inhibition by La^{3+} halted CICR recovery ($n = 7$) whereas in control cells ($n = 8$) Ca^{2+} still returned to baseline (Fig. 6*A*, middle). As with the Na^+-replacement experiment, the post-train stimulus area from 1 to 11 min was not significantly different in La^{3+}-treated neurons, whereas the area from 11 to 21 min post-train stimulus was significantly enhanced (Fig. 6*C*).

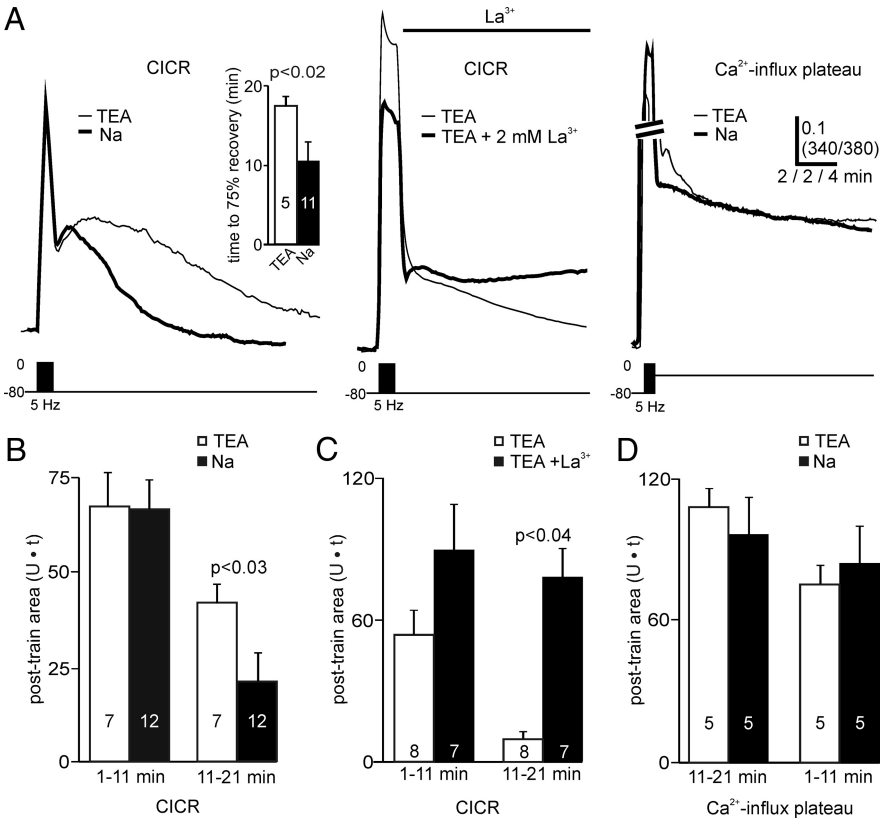

Figure 6. Mitochondrial Ca^{2+} release is removed by the Na^+/Ca^{2+} exchanger and the PMCA. ***A***, Left, In the absence of extracellular Na^+ (TEA, light trace), the mitochondrial Ca^{2+} plateau evoked by a 1 min, 5 Hz train stimulus from −80 mV is prolonged compared with cells bathed in extracellular Na^+ (dark trace). ***A***, Inset, The presence of extracellular Na^+ significantly accelerated the time to 75% recovery for CICR (Mann–Whitney *U* test). ***A***, Middle, In Na^+-free extracellular saline (TEA), the application of La^{3+} (dark trace) during the onset of CICR occludes recovery. In these experiments, cells are voltage-clamped at −80 mV following the stimulus. ***A***, Right, As a control, a 1 min 5 Hz train stimulus from −80 mV, followed by a prolonged step depolarization evokes a Ca^{2+} plateau similar to CICR (at break, a portion of the Ca^{2+} influx is omitted for clarity to emphasize the Ca^{2+} plateau). The recovery of this Ca^{2+}-influx plateau is insensitive to the replacement of extracellular Na^+ (dark trace) for TEA (light trace). For this experiment, neurons are pretreated with 100 μM TPP to prevent any influence of mitochondrial Ca^{2+} release and are recorded with 0 mM intracellular EGTA. ***B***, The post-train stimulus area from 1 to 11 min during mitochondrial Ca^{2+} release is not significantly different between Na^+ and TEA conditions (unpaired Student's *t* test). However, the area from 11 to 21 min is significantly larger in TEA-containing extracellular saline (Mann–Whitney *U* test). ***C***, In the absence of Na^+/Ca^{2+} exchanger activity, the application of 2 mM La^{3+} during CICR does not alter the post-train stimulus area from 1 to 11 min (Mann–Whitney *U* test), but significantly increases the area from 11 to 21 min (Welch corrected Student's *t* test, respectively). ***D***, Area summary data for the Ca^{2+} plateau evoked by post-train stimulus depolarization at (ranging from −10 to −20 mV). Replacing extracellular Na^+ with TEA does not significantly alter the post-train stimulus area from time 1–11 min or 11–21 (Student's *t* test for both).

The activation of Ca^{2+}-dependent processes is highly sensitive to magnitude, duration, and frequency of cytosolic Ca^{2+} change (Clapham, 1995; Berridge et al., 2003). Therefore, the source specific involvement of the Na^+/Ca^{2+} exchanger may be related to the difference between the rapid, large voltage-gated Ca^{2+} influx, and the slow, moderately sized CICR from the mitochondria. To test this, we examined whether a voltage-gated Ca^{2+} influx plateau, that was similar in amplitude and kinetics to CICR, was sensitive to extracellular Na^+. Neurons were stimulated with a 5 Hz, 1 min train stimulus from −80 mV; however, unlike control conditions, cells were immediately voltage-clamped at a potential ranging from −10 to −20 mV for the remainder of the recording. Holding at a depolarized potential produced a steady Ca^{2+} influx comparable to that elicited during CICR. As with rapid, train stimulus-induced voltage-gated Ca^{2+} influx, the inclusion of extracellular Na^+ ($n = 5$) had no apparent effect on the recovery of the slow, persistent voltage-gated Ca^{2+} influx plateau compared with controls ($n = 5$) (Fig. 6*A*, right). The post-train stimulus areas from 1 to 11 min, and 11–21 min were not significantly different between TEA and Na^+ external conditions (Fig. 6*D*).

A model of bag cell neuron Ca^{2+} dynamics recapitulates EGTA-sensitive CICR

The data concerning bag cell neuron Ca^{2+} removal and release after prolonged stimulation provided the information necessary to create a model of Ca^{2+} dynamics. Previous work from bullfrog sympathetic neurons demonstrated that patterns of Ca^{2+} influx and release can be accounted for by a 3 component model consisting of extracellular, cytosolic, and mitochondrial compartments (Friel and Tsien, 1994; Colegrove et al., 2000b). Therefore, the parameter framework from these models was used in this study. Our three-compartment Ca^{2+} model included an extracellular Ca^{2+} influx source (J_{influx}), uptake (J_{uptake}) and release ($J_{release}$) by a mitochondrial store, and plasma membrane Ca^{2+} efflux (J_{efflux}) (Fig. 7*A*, inset). For simplification, extrusion by the PMCA and Na^+/Ca^{2+} exchanger was represented by a single

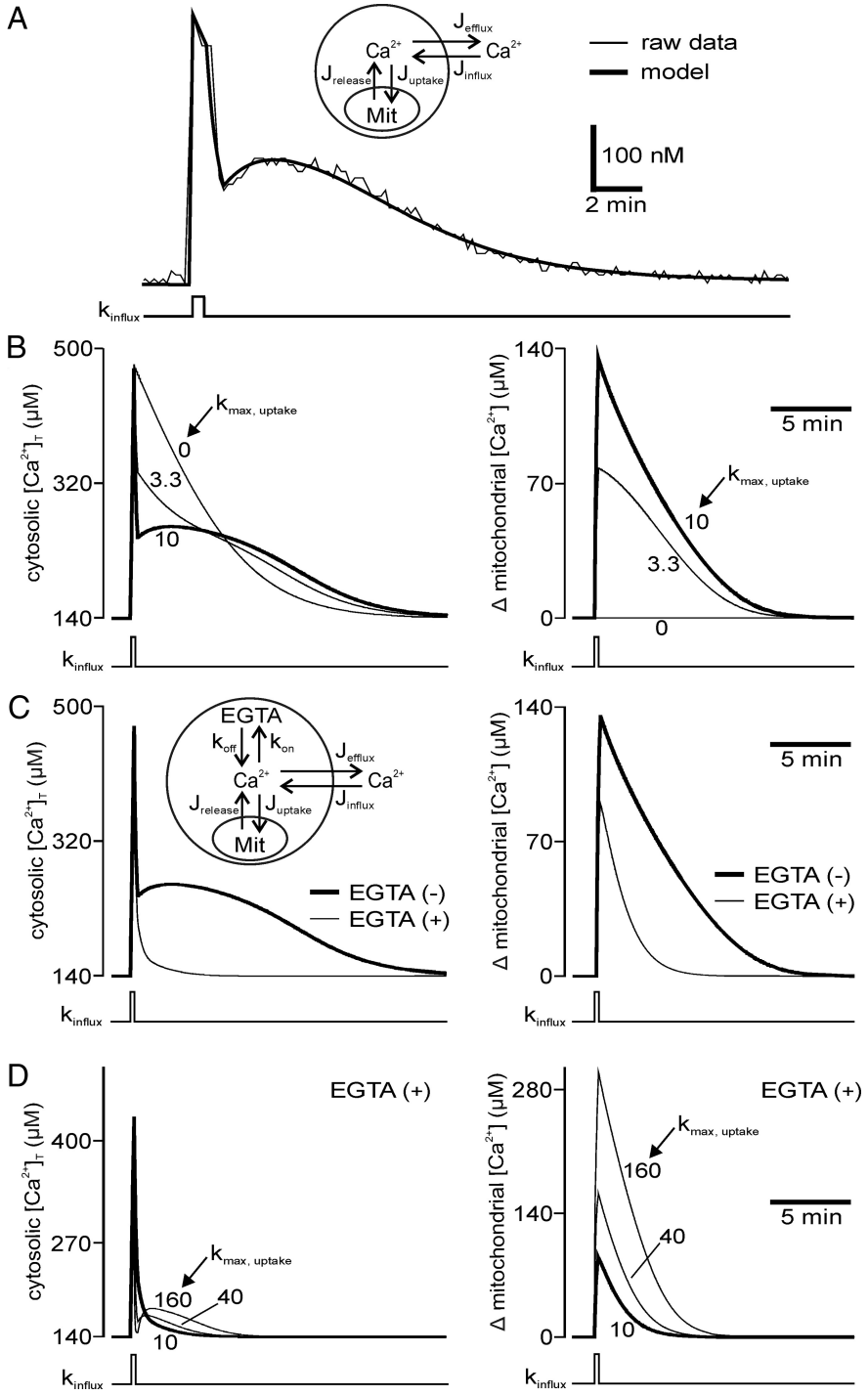

component. Estimates of these rates in the bag cell neurons were derived by fitting raw measurements of free intracellular Ca^{2+} (Fig. 7*A*) (see Materials and Methods). Values derived from individual traces were collected and averaged to produce the model parameters used for the subsequent graphs (Fig. 7*B–D*). To account for the buffering of Ca^{2+} by EGTA, fura, and endogenous Ca^{2+}-binding proteins, rates of free Ca^{2+} removal and extrusion were converted to rates of total Ca^{2+} removal. Thus, the model output is presented as concentrations of total cytosolic Ca^{2+} ($[Ca^{2+}]_T$) (Fig. 7*B–D*) (see Materials and Methods).

Transiently increasing the plasma membrane influx rate constant (k_{influx}), to replicate voltage-gated Ca^{2+} influx, produced a fast increase in cytosolic Ca^{2+}, followed by a rapid recovery and a prolonged cytosolic Ca^{2+} plateau with a similar time course as that seen in actual bag cell neurons (Fig. 7*B*, left). Over the same time period, mitochondrial Ca^{2+} rapidly increased and decayed to prestimulus levels (Fig. 7*B*, right), corresponding to the uptake and release phases of cytosolic Ca^{2+}, respectively. To demonstrate the necessity of mitochondrial Ca^{2+} uptake and release, J_{uptake} was tempered by serially reducing the uptake rate constant ($k_{max,uptake}$). This produced a progressively smaller Ca^{2+} increase in the mitochondria, slowed the rate of cytosolic Ca^{2+} removal from peak influx, and reduced the CICR magnitude (Fig. 7*B*, left). These results are qualitatively similar to those seen in ours and other experiments when mitochondrial uptake is eliminated (Thayer and Miller, 1990; Friel and Tsien, 1994; Colegrove et al., 2000a; Geiger and Magoski, 2008).

Figure 7. A model of bag cell neuron Ca^{2+} dynamics demonstrates the sensitivity of mitochondrial Ca^{2+} release to the Ca^{2+} chelating agent, EGTA. ***A***, The inset illustrates the components involved in the 3 compartment model of Ca^{2+}. Ca^{2+} influx is represented by J_{influx}, cytosolic Ca^{2+} removal is mediated by mitochondrial uptake (J_{uptake}) or plasma membrane efflux (J_{efflux}), and mitochondrial Ca^{2+} release is denoted as $J_{release}$. Collectively, these variables determine the cytosolic and mitochondrial Ca^{2+} concentrations (see Materials and Methods). Raw data from a bag cell neuron (light trace) presenting stimulus-induced Ca^{2+} influx, CICR, and recovery is fit by the model (dark trace) to estimate values for free intracellular Ca^{2+} fluxes. Train stimulus-induced Ca^{2+} influx (bottom) is simulated in the model by transiently increasing the Ca^{2+} influx rate constant (k_{influx}). Directly after reducing k_{influx} there is a rapid recovery leading to a prolonged Ca^{2+} plateau that readily fits the raw data (root mean square error: 2.3×10^{-8}). Parameters for this fit are (± 95% confidence interval): $V_{max,\ efflux}$: 6.2 ± 0.26 nM/s, $k_{max,\ uptake}$: 4.45 ± 0.82 (s^{-1}), $V_{max,\ release}$: 6.2 ± 1.14 nM/s. Unless otherwise stated, all subsequent model presentations were derived using the average values presented in Table 1. The values in Table 1 reflect parameters measured from changes to free Ca^{2+}, before converting to rates of total Ca^{2+}. ***B***, For this and subsequent model graphs, Ca^{2+} levels reflect total, rather than free intracellular Ca^{2+} to correct for the presence of exogenous (fura and/or EGTA) and endogenous Ca^{2+} buffers present when estimating rates (see Materials and Methods). Serially reducing the rate constant of mitochondrial Ca^{2+} uptake ($k_{max,\ uptake}$) from 10 to 3.3 then 0 (s^{-1}) attenuates the degree of mitochondrial Ca^{2+} uptake (right, light traces), slows the post-stimulus removal, and reduces CICR (left, light traces). ***C***, Left inset, to include EGTA (0.5 mM), the bag cell neuron model of Ca^{2+} dynamics is increased to four components by adding Ca^{2+} removal by an exogenous Ca^{2+} binding agent. The clearance of Ca^{2+} by EGTA is determined by its forward (k_{on}) and reverse (k_{off}) rate constants, respectively. In the absence of EGTA, evoking Ca^{2+} influx causes a rise in Ca^{2+} and a subsequent Ca^{2+} plateau (left, dark trace). Under these conditions, mitochondrial Ca^{2+} increases then falls as Ca^{2+} is released into the cytosol (right, dark trace). The cytosolic Ca^{2+} response in the presence of EGTA slightly reduces peak Ca^{2+} influx magnitude and eliminates mitochondrial CICR (left, light traces). EGTA also partially attenuates the magnitude of mitochondrial Ca^{2+} influx after stimulation (right, light traces). ***D***, In the presence of an EGTA component (0.5 mM), increasing the mitochondrial uptake rate constant ($k_{max,\ uptake}$) from 10 to 40 then 160 (s^{-1}), potentiates the degree of mitochondrial Ca^{2+} loading (right, light traces), speeds the rate of cytosolic Ca^{2+} recovery after influx, and produces very limited CICR (left, light traces).

Having established parameters that replicate our experiments, we sought to address the sensitivity of CICR to intracellular EGTA. The effects of EGTA on CICR could be due to competition with mitochondrial uptake for Ca^{2+} influx, causing a reduction in mitochondrial loading and subsequent release, or by EGTA binding the Ca^{2+} as it is extruded. To discern between these possibilities, a fourth component was added to the model, representing the buffering of Ca^{2+} by EGTA, which was determined by its forward (k_{on}) and reverse reaction rate constants (k_{off}; see Materials and Methods) (Nowycky and Pinter, 1993; Naraghi, 1997). Inclusion of an EGTA component (0.5 mM) in the compartment model caused a small reduction in the peak cytosolic Ca^{2+} rise during influx, while eliminating CICR (Fig. 7*C*, left). This *in silico* result is strikingly comparable to that observed *in vitro* (Fig. 1). In the EGTA-containing conditions, peak mitochondrial Ca^{2+} levels were slightly reduced following cytosolic Ca^{2+} influx, and consequently, decayed to prestimulus Ca^{2+} levels at a faster time course than in the absence of EGTA (Fig. 7*C*, right).

To determine whether increasing the degree of mitochondrial Ca^{2+} loading could rescue CICR in the presence of the EGTA component (0.5 mM), mitochondrial uptake was serially enhanced. Stepping the $k_{max,\ uptake}$ from our standard value of 10 to 40 then 160 (s^{-1}) increased mitochondrial Ca^{2+} to concentrations as large or higher than those seen in the absence of EGTA (compare Fig. 7*C*, right, *D*, right). Despite increasing the degree of mitochondrial Ca^{2+} available for release by enhancing mitochondrial uptake, CICR was only weakly rescued in the presence of EGTA. Thus, the sensitivity of CICR to EGTA is largely attributable to competition for Ca^{2+} released from the mitochondria.

Store-operated Ca^{2+} influx refills the ER Ca^{2+} store and is primarily cleared by the SERCA

In addition to voltage-gated Ca^{2+} influx and CICR, a third Ca^{2+} source prominent in the bag cell neurons is store-operated Ca^{2+} influx (Kachoei et al., 2006). It is well established that signaling cascades release ER Ca^{2+} through ryanodine- and inositol triphospate (IP_3)-receptors in the bag cell neurons (Fink et al., 1988; Fisher et al., 1994; Geiger and Magoski, 2008). Here we evoked store-operated influx to determine whether a third Ca^{2+} source uses distinct removal mechanisms.

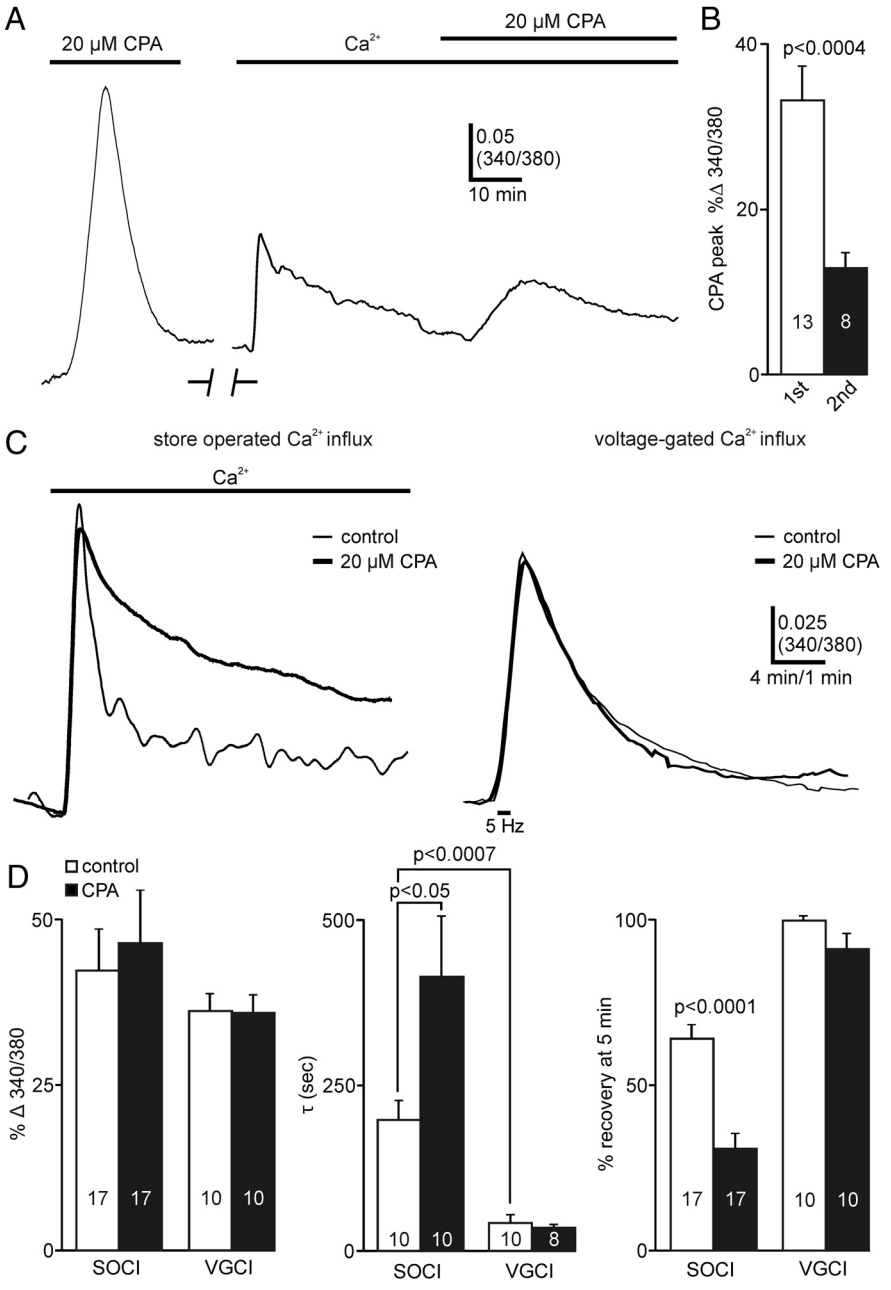

Figure 8. The store-operated Ca^{2+} influx pathway is cleared by the SERCA to replete the ER. ***A***, Addition of 20 μM CPA depletes ER Ca^{2+} in a cultured bag cell neuron pressure-injected with fura-PE3. Because neurons are not recorded under voltage clamp, a normal Na^{+}-containing and K^{+}-containing external solution is used. After the first depletion, CPA is washed out using bath exchange (at break); upon recording resumption, the addition of extracellular Ca^{2+} results in a rapid elevation of intracellular Ca^{2+}. Delivering CPA a second time again evokes a Ca^{2+} rise, albeit smaller than the first, indicating repletion of the CPA-sensitive store. ***B***, The magnitude of Ca^{2+} release to the second CPA exposure, after store-operated influx, is significantly smaller than the response elicited during the first CPA-induced depletion (unpaired Student's *t* test). ***C***, Left, Washout of CPA, before addition of extracellular Ca^{2+}, speeds the recovery of influx back to baseline. The removal of store-operated Ca^{2+} recovers at a slower rate in the presence of CPA (dark trace). Both neurons previously depleted in Ca^{2+}-free ASW with 20 μM CPA. ***C***, Right, Ca^{2+} influx, similar in size to that evoked by store-operated influx, caused by a short 5 Hz train of depolarizing stimuli from −80 to 0 mV in the presence (dark trace) and absence (light trace) of CPA. CPA has no effect on the speed of recovery from the short stimulus. ***D***, Left, Mean percentage change in 340/380 (left) indicates that the increase in cytosolic Ca^{2+} during store-operated Ca^{2+} influx and the short train stimulus Ca^{2+} influx are not significantly different within and between conditions (ANOVA). ***D***, Middle, CPA significantly increases the mean store-operated Ca^{2+} influx decay time constant (Welch corrected unpaired Student's *t* test) although having no effect on the mean τ of the similarly sized train stimulus-induced Ca^{2+} influx (unpaired Student's *t* test). ***D***, Right, The percentage recovery at 5 min (right) after the application of extracellular Ca^{2+} is significantly shorter with prior CPA washout (Welch corrected unpaired Student's *t* test). However, the percentage recovery at 5 min after the short train stimulus Ca^{2+} influx is not significantly altered by CPA.

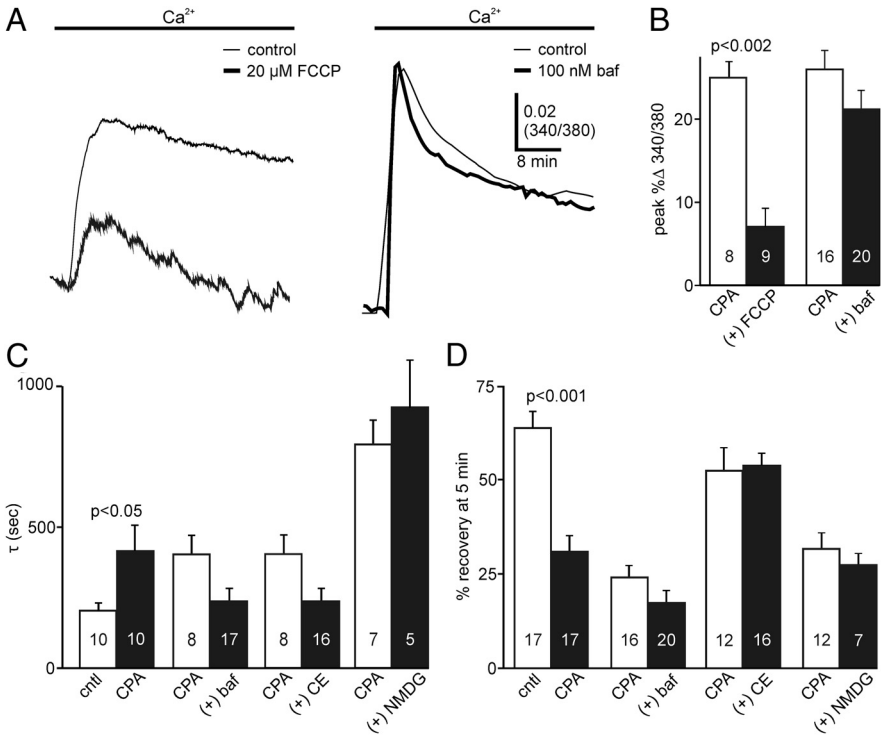

Figure 9. Store-operated Ca^{2+} influx is reduced in magnitude by FCCP but is not influenced by acidic stores, the PMCA, or the Na^{+}/Ca^{2+} exchanger. ***A***, Left, Neurons exposed to 20 μM FCCP before the addition of extracellular Ca^{2+} (dark trace) causes a reduction in store-operated influx relative to control (light trace). ***A***, Right, Exposure to 100 nM bafilomycin A (baf) before the addition of extracellular Ca^{2+} (dark trace) does not influence the size or recovery of store-operated Ca^{2+} influx. Neurons were previously depleted in Ca^{2+}-free ASW with 20 μM CPA. ***B***, Treatment with FCCP significantly reduces the peak Ca^{2+} influx after the addition of extracellular Ca^{2+} (left), whereas bafilomycin has no effect (both comparisons using Mann–Whitney *U* test). ***C***, Summary data demonstrating that the mean decay time constant (τ) is significantly larger in CPA (Welch corrected unpaired Student's *t* test), but not in bafilomycin (unpaired Student's *t* test), 20 μM carboxyeosin (CE) (Welch corrected Student's *t* test), or where extracellular Na^{+} is replaced with NMDG (Mann–Whitney *U* test). ***D***, CPA pretreatment significantly reduces the percentage recovery from peak Ca^{2+}, whereas incubation with bafilomycin, carboxyeosin, or extracellular NMDG does not (all comparisons using unpaired Student's *t* test).

To measure store-operated Ca^{2+} influx, bag cell neurons were fura-filled by sharp-electrode pressure injection rather than recorded under whole-cell voltage clamp. This was possible because ER depletion and store-operated Ca^{2+} influx do not significantly alter the membrane potential, and therefore do not require voltage clamp (Kachoei et al., 2006). Store-operated influx was activated by applying 20 μM CPA in Ca^{2+}-free medium to deplete the ER by inhibiting the SERCA (Seidler et al., 1989). After depletion and washout of CPA, the addition of Ca^{2+} back to the bath caused a rapid rise in intracellular Ca^{2+} as a result of Ca^{2+} influx through depletion-activated store-operated channels (Fig. 8*A*). A second application of CPA after influx and recovery elicited another rise in intracellular Ca^{2+} (Fig. 8*A*); however, its magnitude was significantly smaller than the first (Fig. 8*B*). In contrast, when store-operated influx recovery occurred in the presence of CPA (see below), a second application of CPA had no apparent effect on resting Ca^{2+} (data not shown).

These results indicate that store-operated Ca^{2+} influx refills the ER via the SERCA. To determine the degree of Ca^{2+} removal by the SERCA, the recovery from peak store-operated Ca^{2+} influx was measured in the presence and absence of CPA. After ER depletion, washout of CPA and addition of extracellular Ca^{2+} evoked a transient rise in Ca^{2+} followed by a monoexponential decay, typically reaching pre-influx baseline within 10 min (Fig. 8*C*, left). If CPA remained in the bath after depletion ($n = 17$), store-operated influx was similar in size compared with controls ($n = 17$); however, Ca^{2+} recovery slowed dramatically, often requiring well over 15 min for full recovery (Fig. 8*C*, left). Furthermore, in CPA, following a brief initial recovery, Ca^{2+} levels often decayed to a new baseline at a Ca^{2+} concentration higher than pre-influx levels.

Our previous data established that the ER was ineffective at removing rapid voltage-gated Ca^{2+} influx. As the activity of the SERCA pump was demonstrated to be a relatively slow during store-operated influx, the effect of CPA on the recovery of a large Ca^{2+} influx may have gone undetected. Therefore, we produced a voltage-gated Ca^{2+} influx, sized-matched to the average store-operated influx, and tested its sensitivity to CPA (control $n = 10$, CPA $n = 10$). A brief (1.5–3 s) 5 Hz train stimulus from −80 to 0 mV applied to fura-loaded bag cell neurons under whole-cell voltage clamp elicited response magnitudes that were not significantly different than those during store-operated influx (Fig. 8*D*, left). Despite having the same absolute magnitude as store-operated influx, voltage-gated Ca^{2+} influx had a dramatically faster exponential recovery (Fig. 8*D*, middle). Consistent with this, the handling of voltage-gated Ca^{2+} influx showed no sensitivity to CPA, and rapidly declined to prestimulus levels within 2 min (Fig. 8*C*, right, *D*, middle, right).

Role for the mitochondria, but not the PMCA or Na^{+}/Ca^{2+} exchanger, in store-operated Ca^{2+} influx

In other systems, mitochondria have been shown to be functionally coupled to store-operated influx (Gilabert and Parekh, 2000; Glitsch et al., 2002; Parekh and Putney, 2005; Naghdi et al., 2010). Therefore, influx was measured after 20 min pretreatment with 20 μM FCCP, to collapse the mitochondrial membrane potential. Compared with controls ($n = 8$), FCCP-treated neurons ($n = 9$) had a significantly reduced peak percentage change in response to bath application of Ca^{2+} after CPA-induced depletion (Fig. 9*A*, left, *B*). Furthermore, exposure to FCCP reduced the percentage of cells presenting a measurable influx signal. In the DMSO-treated group, 8 of 9 cells showed a response, whereas after FCCP, influx was observed only in 9 of 24 neurons ($p < 0.02$, Fisher's exact test). The contribution of acidic stores to the removal of store-operated influx was tested by exposing cells with 100 nM bafilomycin A (Fig. 9*A*, right). Incubation in bafilomycin A ($n = 20$) before the addition of extracellular Ca^{2+} did not change the peak store-operated influx (Fig. 9*B*), Ca^{2+} decay time constant (Fig. 9*C*), or the percentage recovery at 5 min post-peak Ca^{2+} compared with control ($n = 16$) (Fig. 9*D*).

Contributions from the Na^{+}/Ca^{2+} exchanger and the PMCA were examined by including extracellular NMDG in lieu of Na^{+} and 20 μM carboxyeosin, respectively. We used NMDG to inhibit

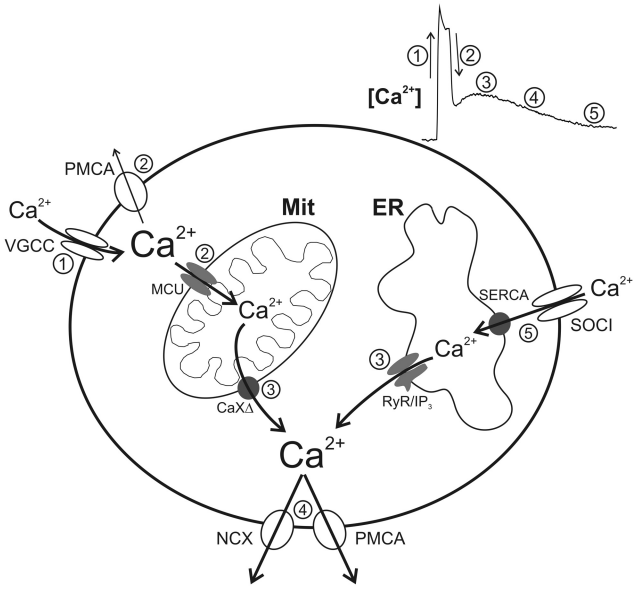

Figure 10. Ca^{2+} from multiple sources is cleared by distinct sets of Ca^{2+} removal systems in the bag cell neurons. A conceptual model of Ca^{2+} dynamics during an afterdischarge based on the current study and prior work by our laboratory and others (Fink et al., 1988; Fisher et al., 1994; Michel and Wayne, 2002; Kachoei et al., 2006; Geiger and Magoski, 2008). Top, right inset, A sample trace of intracellular Ca^{2+} presumed to reflect afterdischarge dynamics *in vivo*. Numbers correspond to a series of chronological events depicted in the main illustration: ***1***, During the fast phase of the afterdischarge there is a large Ca^{2+} influx through action potential-evoked voltage-gated Ca^{2+} channels (VGCC). ***2***, This early Ca^{2+} influx is predominantly removed by rapid mitochondrial uptake, with ancillary assistance from the PMCA. ***3***, Ca^{2+} accumulates in the mitochondria, after which it is slowly extruded into the cytosol through a TPP-sensitive Ca^{2+}-exchanger. Additionally, second messenger cascades are activated that initiate Ca^{2+} liberation from the ER through IP_3 and ryanodine receptors. ***4***, The release of Ca^{2+} from intracellular stores causes a prolonged rise in cytosolic Ca^{2+} that is removed by the Na^+/Ca^{2+} exchanger and the PMCA. ***5***, Last, sustained Ca^{2+} release during the afterdischarge depletes the ER and initiates store-operated Ca^{2+} influx: a distinct Ca^{2+} source that is removed by the SERCA into the ER lumen.

the Na^+/Ca^{2+} exchanger (Blaustein and Lederer, 1999; Zhang et al., 2004), rather than TEA, because TEA blocks K^+ currents and would depolarize bag cell neurons in non-voltage-clamped conditions (Hagiwara and Saito, 1959; Kaczmarek and Strumwasser, 1984). Carboxyeosin, a different PMCA inhibitor (Shmigol et al., 1998), was used because the onset time of store-operated influx varied among individual cells during a recording, making proper timing of La^{3+} application impossible. Again, SERCA function was inhibited by 20 μM CPA following prior ER depletion. Blocking the Na^+/Ca^{2+} exchanger (Na^+ $n = 12$; NMDG $n = 7$) or the PMCA (control $n = 12$; carboxyeosin $n = 16$) did not significantly alter the decay time constants (Fig. 9*C*) or the percentage recovery at 5 min (Fig. 9*D*) despite the ongoing presence of CPA.

Discussion

Although neuron-specific or compartment-specific expression of Ca^{2+} clearance systems has been reported, there is sparse evidence of differential handling mechanisms between Ca^{2+} sources. White and Reynolds (1995) found that a glutamate-evoked Ca^{2+} response is more sensitive to the disruption of the Na^+/Ca^{2+} exchanger and mitochondria than voltage-gated Ca^{2+} influx. Conversely, in mouse taste receptor cells voltage-gated Ca^{2+} influx, but not Ca^{2+} release, is Na^+/Ca^{2+} exchanger sensitive (Szebenyi et al., 2010). This work is the first to fully characterize the disparate contribution of handling mechanisms to multiple Ca^{2+} sources in a single neuronal species. We demonstrate: (1) voltage-gated Ca^{2+} influx is primarily removed by the mitochondria with a secondary contribution from the PMCA; (2) CICR arises from subsequent mitochondrial Ca^{2+} release, which is then handled by the Na^+/Ca^{2+} exchanger and the PMCA; and (3) store-operated Ca^{2+} influx is sequestered via the SERCA (Fig. 10). This is profound, given that each Ca^{2+} source provides unique contributions to neuronal function.

Voltage-gated Ca^{2+} entry is the primary means to increase cytosolic Ca^{2+} (Catterall and Few, 2008). In the bag cell neurons, this gates Ca^{2+}-dependent cation channels that promote the afterdischarge (Whim and Kaczmarek, 1998; Lupinsky and Magoski, 2006; Hung and Magoski, 2007). We show that voltage-gated Ca^{2+} influx is handled by the mitochondria, similar to some neurons and neuroendocrine cells (Werth and Thayer, 1994; Kaftan et al., 2000). However, unlike chromaffin cells, where mitochondrial uptake is engaged only at high Ca^{2+} (Herrington et al., 1996), bag cell neuron mitochondria function near resting and peak Ca^{2+} levels. Neuroendocrine cells provide hormones to orchestrate fundamental behaviors, such as feeding, drinking, and reproduction (Arnauld et al., 1974; Lincoln and Wakerley, 1974; Kawakami et al., 1982). Considering the importance of energy status to these behaviors, it is unsurprising that mitochondria are the first recipients of Ca^{2+} during bag cell neuron excitation. Essentially, mitochondria are situated to act as gatekeepers of the afterdischarge and reproductive status.

In the bag cell neurons, a 1 min stimulus evoked CICR that is sensitive to TPP or intracellular EGTA. A compartment model of bag cell neuron Ca^{2+} suggests that the effect of EGTA on CICR was partially due to a reduction in mitochondrial Ca^{2+} loading, but mainly the result of EGTA binding extruded mitochondrial Ca^{2+}. Likely, this is possible because of slow Ca^{2+} release versus fast uptake across the mitochondria. Similarly, maximal uptake in sympathetic neuron mitochondria approaches ~120 nM/s, whereas release is far slower (~35 nM/s) (Colegrove et al., 2000a). Such kinetics render mitochondrial Ca^{2+} release sensitive to competitive cytoplasmic buffers. CICR transduces short-lived events into protracted Ca^{2+} signals, which impact biochemical pathways more effectively than the initial response alone. For example, CICR promotes posttetanic transmitter release at mouse neuromuscular junctions and hippocampal synapses (Garcia-Chacon et al., 2006; Lee et al., 2007), and prolongs Ca^{2+}-dependent transcription in dorsal root ganglion neurons (Kim and Usachev, 2009). During an afterdischarge, CICR may serve analogously to sustain hormone release. Indeed, some ELH secretion is independent of extracellular Ca^{2+}, implicating the involvement of Ca^{2+} stores (Wayne et al., 1998; Michel and Wayne, 2002). The prolonged duration of bag cell neuron CICR reflects a combination of persistent Ca^{2+} release, and removal by the PMCA and Na^+/Ca^{2+} exchanger, providing an efficient form of recycling Ca^{2+} to the extracellular space. These extrusion mechanisms, which are slow (~4 nM/s), may shape CICR but not necessarily dampen its effectiveness. The mitochondria cope with Ca^{2+} influx and transduce it into a lengthy release that is extruded without saturating the maximal rate of plasma membrane transport.

Store-operated Ca^{2+} influx was exclusively handled by the SERCA. Accordingly, this pump refilled the ER, consistent with similar roles of store-operated Ca^{2+} influx in other cells (Hoth and Penner, 1992; Putney, 2003). In the bag cell neurons, ER Ca^{2+} release occurs via IP_3 and ryanodine receptors, and can activate a BK-like K^+ channel and cation current (Fink et al., 1988; Knox et al., 1996) and may contribute to ELH secretion (Michel and Wayne, 2002). Activation of store-operated influx

requires ER depletion. As such, it likely presents a delayed activation, once the majority of Ca^{2+} liberation has occurred (Fig. 10), and could sustain processes activated by ER Ca^{2+}. Store-operated influx was also reduced when mitochondrial function was absent. This is also seen in T-lymphocytes and retinoblastoma-1 cells, where mitochondrial Ca^{2+} sequestration prevents Ca^{2+}-dependent inhibition of store-operated channels (Glitsch et al., 2002; Naghdi et al., 2010). In the bag cell neurons, although neither the Na^+/Ca^{2+} exchanger nor the PMCA were involved, there was a residual recovery from peak store-operated influx when the SERCA was inhibited. Therefore, a similar explanation involving mitochondrial Ca^{2+} clearance is plausible.

The specificity between Ca^{2+} sources and clearance mechanisms seen in this study could be attributed to the duration of Ca^{2+} exposure, the affinity of the Ca^{2+} handling systems, and/or the distribution of the buffers and influx sources (Gabso et al., 1997; Berridge et al., 2003). The proportion of removal by each handling mechanism depends on influx magnitude. For example, the PMCA and SERCA are reported to have high Ca^{2+}-binding affinities and remove small Ca^{2+} loads, whereas the low affinity Na^+/Ca^{2+} exchanger and mitochondria are engaged only by high intracellular Ca^{2+} (Herrington et al., 1996; Blaustein and Lederer, 1999; Berridge et al., 2003). Such is not the case here, where voltage-gated Ca^{2+} influx of similar size as store-operated influx or CICR does not engage the Na^+/Ca^{2+} exchanger or SERCA. This is also confirmed by our prior work demonstrating the CPA-insensitivity of a small voltage-gated Ca^{2+} influx elicited in sharp-electrode recorded bag cell neurons (Geiger and Magoski, 2008). It is doubtful that differences in Ca^{2+} signal kinetics contributed to our results. A prolonged poststimulus Ca^{2+} influx showed no sensitivity to the Na^+/Ca^{2+} exchanger, despite demonstrating a similar duration as CICR. Furthermore, CICR occurred with a duration and magnitude comparable to store-operated Ca^{2+} influx, and yet presented a different involvement of the SERCA, PMCA, and Na^+/Ca^{2+} exchanger. Thus, the differential control we observe seems attributable to variation in the location of Ca^{2+} sources and/or handling systems. Indeed, Ca^{2+} channel types, including those in the bag cell neurons, can occupy discrete areas within the soma (White and Kaczmarek, 1997). Furthermore, in cortical neurons and astrocytes, the Na^+/Ca^{2+} exchanger parallels the position of intracellular organelles and can occupy distinct regions relative to the PMCA (Juhaszova et al., 1996, 2000). Organelles can also occupy unique cellular loci. In bullfrog sympathetic neurons, SERCA clusters near the plasma membrane, whereas the mitochondria form a centralized inner ring (McDonough et al., 2000). Preferential localization can have functional implications, such as in cervical ganglion neurons, where Ca^{2+} handling is biased toward a given source, by the ER and mitochondria associating with Ca_v2 but not Ca_v1 channels (Wheeler et al., 2012).

Unlike in the calyx of Held and retinal bipolar cells (Zenisek and Mathews, 2000; Kim et al., 2005), we find that, in the absence of a dominant removal system, the contribution of an otherwise uninvolved clearance mechanism is not enhanced. Compensation likely occurs because Ca^{2+} gradients disperse after influx (Hua et al., 1993), diffusing to buffers that are displaced from the source. Therefore, even when considering a heterogeneous distribution of removal systems, our results are surprising. Potentially, Ca^{2+} signals are compartmentalized by diffusional barriers such as partitions formed by membrane junctions (e.g., ER-plasma membrane) (Carrasco and Meyer, 2011) or "Ca^{2+}-sponging" by immobile Ca^{2+}-binding proteins (Nowycky and Pinter, 1993; Weiss et al., 2012), which are found in other *Aplysia* neurons. Estimates of the Ca^{2+}-diffusion coefficient in cultured *Aplysia* neurons ($\leq 16\ \mu m^2/s$) are similar to those of specialized Ca^{2+} signaling structures, such as dendrites (10–50 $\mu m^2/s$) or photoreceptor outer segments (15 $\mu m^2/s$) (Gabso et al., 1997; Murthy et al., 2000; Nakatani et al., 2002). Therefore, auxiliary systems may have contributed to removal, but their effects were slow or delayed.

Although differential clearance between sources may reflect an efficient form of Ca^{2+} homeostasis or Ca^{2+}-metabolism coupling (Rizzuto et al., 1998; Chouhan et al., 2012), a more intriguing possibility is that it shapes Ca^{2+} signals to determine which Ca^{2+}-dependent pathway is activated. In the aforementioned superior cervical ganglion neurons, the mitochondria and ER preferentially remove Ca^{2+} influx from Ca_v2, but not Ca_v1 channels, permitting Ca_v1-specific activation of transcription (Wheeler et al., 2012). For bag cell neurons, Ca^{2+} entry through a cation channel, but not voltage-gated Ca^{2+} influx or Ca^{2+} release, induces a period of refractoriness to further stimulation (Magoski et al., 2000). Furthermore, following the afterdischarge, there is a Ca^{2+}-influx-dependent increase in ELH synthesis, which could be brought about by differences in the clearance of Ca^{2+} from distinct sources (Wayne et al., 2004). Differential handling between Ca^{2+} sources could underlie the ability of discrete Ca^{2+} sources to activate specific downstream targets. Our work reinforces the shifting view of Ca^{2+} buffers as passive determinants of intracellular Ca^{2+} to dynamic regulators that can control excitability, secretion, synaptic plasticity, and gene expression (Krizaj and Copenhagen, 1998; Holthoff et al., 2002; Kim and Usachev, 2009; Simons et al., 2009).

References

Arch S (1972) Polypeptide secretion from the isolated parietovisceral ganglion of *Aplysia californica*. J Gen Physiol 59:47–59. CrossRef Medline

Armstrong CM, Hille B (1998) Voltage-gated ion channels and electrical excitability. Neuron 20:371–380. CrossRef Medline

Arnauld E, Vincent JD, Dreifuss JJ (1974) Firing patterns of hypothalamic supraoptic neurons during water deprivation in monkeys. Science 185:535–537. CrossRef Medline

Babcock DF, Herrington J, Goodwin PC, Park YB, Hille B (1997) Mitochondrial participation in the intracellular Ca^{2+} network. J Cell Biol 136:833–844. CrossRef Medline

Berridge MJ, Lipp P, Bootman MD (2000) The versatility and universality of calcium signaling. Nat Rev Mol Cell Biol 1:11–21. CrossRef Medline

Berridge MJ, Bootman MD, Roderick HL (2003) Calcium signalling: dynamics, homeostasis and remodelling. Nat Rev Mol Cell Biol 4:517–529. CrossRef Medline

Blaustein MP, Lederer JW (1999) Sodium/calcium exchange: its physiological implications. Physiol Rev 79:763–854. Medline

Bowman EJ, Siebers A, Altendorf K (1988) Bafilomycins: a class of inhibitors of membrane ATPases from microorganisms, animal cells, and plant cells. Proc Natl Acad Sci U S A 85:7972–7976. CrossRef Medline

Carafoli E (1991) Calcium pump of the plasma membrane. Physiol Rev 71:129–153. Medline

Caride AJ, Filoteo AG, Penheiter AR, Pászty K, Enyedi A, Penniston JT (2001) Delayed activation of the plasma membrane calcium pump by a sudden increase in Ca^{2+}: fast pumps reside in fast cells. Cell Calcium 30:49–57. CrossRef Medline

Carrasco S, Meyer T (2011) STIM proteins and the endoplasmic reticulum-plasma membrane junctions. Annu Rev Biochem 80:973–1000. CrossRef Medline

Catterall WA, Few AP (2008) Calcium channel regulation and presynaptic plasticity. Neuron 59:882–901. CrossRef Medline

Chouhan AK, Ivannikov MV, Lu Z, Sugimori M, Llinas RR, Macleod GT (2012) Cytosolic calcium coordinates mitochondrial energy metabolism with presynaptic activity. J Neurosci 32:1233–1243. CrossRef Medline

Christensen KA, Myers JT, Swanson JA (2002) pH-dependent regulation of lysosomal calcium in macrophages. J Cell Sci 115:599–607. Medline

Clapham DE (1995) Calcium signaling. Cell 80:259–268. CrossRef Medline

Colegrove SL, Albrecht MA, Friel DD (2000a) Dissection of mitochondrial Ca^{2+} uptake and release fluxes *in situ* after depolarization evoked $[Ca^{2+}]_i$ elevations in sympathetic neurons. J Gen Physiol 115:351–370. CrossRef Medline

Colegrove SL, Albrecht MA, Friel DD (2000b) Quantitative analysis of mitochondrial Ca^{2+} uptake and release pathways in sympathetic neurons. Reconstruction of the recovery after depolarization-evoked $[Ca^{2+}]_i$ elevations. J Gen Physiol 115:381–388. CrossRef Medline

Deisseroth K, Heist EK, Tsien RW (1998) Translocation of calmodulin to the nucleus supports CREB phosphorylation in hippocampal neurons. Nature 392:198–202. CrossRef Medline

DeRiemer SA, Kaczmarek LK, Lai Y, McGuinness TL, Greengard P (1984) Calcium/calmodulin-dependent protein phosphorylation in the nervous system of *Aplysia.* J Neurosci 4:1618–1625. Medline

Fierro L, DiPolo R, Larno I (1998) Intracellular calcium clearance in Purkinje cell somata from rat cerebellar slices. J Physiol 510:499–512. CrossRef Medline

Fink LA, Connor JA, Kaczmarek LK (1988) Inositol triphosphate releases intracellularly stored calcium and modulates ion channels in molluscan neurons. J Neurosci 8:2544–2555. Medline

Fisher TE, Levy S, Kaczmarek LK (1994) Transient changes in intracellular calcium associated with a prolonged increase in excitability in neurons of *Aplysia californica.* J Neurophysiol 71:1254–1257. Medline

Friel DD, Tsien RW (1994) An FCCP-sensitive Ca^{2+} store in bullfrog sympathetic neurons and its participation in stimulus-evoked changes in $[Ca^{2+}]_i$. J Neurosci 14:4007–4024. Medline

Gabso M, Neher E, Spira ME (1997) Low mobility of the Ca^{2+} buffers in axons of cultured *Aplysia* neurons. Neuron 18:473–481. CrossRef Medline

García-Chacón LE, Nguyen KT, David G, Barrett EF (2006) Extrusion of Ca^{2+} from mouse motor terminal mitochondria via a Na^+-Ca^{2+} exchanger increases post-tetanic evoked release. J Physiol 574:663–675. CrossRef Medline

Gardam KE, Geiger JE, Hickey CM, Hung AY, Magoski NS (2008) Flufenamic acid affects multiple currents and causes intracellular Ca^{2+} release in *Aplysia* bag cell neurons. J Neurophysiol 100:38–49. CrossRef Medline

Geiger JE, Magoski NS (2008) Ca^{2+}-induced Ca^{2+}-release in *Aplysia* bag cell neurons requires interaction between mitochondrial and endoplasmic reticulum stores. J Neurophysiol 100:24–37. CrossRef Medline

Gilabert JA, Parekh AB (2000) Respiring mitochondria determine the pattern of activation and inactivation of the store-operated Ca^{2+} current I_{CRAC}. EMBO J 19:6401–6407. CrossRef Medline

Glitsch MD, Bakowski D, Parekh AB (2002) Store-operated Ca^{2+} entry depends on mitochondrial Ca^{2+} uptake. EMBO J 21:6744–6754. CrossRef Medline

Gonçalves PP, Meireles SM, Neves P, Vale MG (1999) Synaptic vesicle Ca^{2+}/H^+ antiport: dependence on the proton electrochemical gradient. Mol Brain Res 71:178–184. CrossRef Medline

Gorman AL, Thomas MV (1980) Intracellular calcium accumulation during depolarization in a molluscan neuron. J Physiol 308:259–285. Medline

Grynkiewicz G, Poenie M, Tsien RY (1985) A new generation of Ca^{2+} indicators with greatly improved fluorescence properties. J Biol Chem 260:3440–3450. Medline

Gunter KK, Gunter TE (1994) Transport of calcium by mitochondria. J Bioenerg Biomembr 26:471–485. CrossRef Medline

Gunter TE, Pfeiffer DR (1990) Mechanisms by which mitochondria transport calcium. Am J Physiol 258:755–786. Medline

Hagiwara S, Saito N (1959) Voltage-current relations in nerve cell membrane of *Onchidium verruculatum.* J Physiol 148:161–179. Medline

Herrington J, Park YB, Babcock DF, Hille B (1996) Dominant role of mitochondria in clearance of large Ca^{2+} loads from rat adrenal chromaffin cells. Neuron 16:219–228. CrossRef Medline

Heytler PG, Prichard WW (1962) A new class of uncoupling agents–carbonyl cyanide phenylhydrazones. Biochem Biophys Res Commun 7:272–275. CrossRef Medline

Hickey CM, Geiger JE, Groten CJ, Magoski NS (2010) Mitochondrial Ca^{2+} activates a cation current in *Aplysia* bag cell neurons. J Neurophysiol 103:1543–1556. CrossRef Medline

Holthoff K, Tsay D, Yuste R (2002) Calcium dynamics of spines depend on their dendritic location. Neuron 33:425–437. CrossRef Medline

Hoth M, Penner R (1992) Depletion of intracellular calcium stores activates a calcium current in mast cells. Nature 355:353–356. CrossRef Medline

Hua SY, Nohmi M, Kuba K (1993) Characteristics of Ca^{2+} release induced by Ca^{2+} influx in cultured bullfrog sympathetic neurons. J Physiol 464:245–272. Medline

Hung AY, Magoski NS (2007) Activity-dependent initiation of a prolonged depolarization in *Aplysia* bag cell neurons: role for a cation channel. J Neurophysiol 97:2465–2479. CrossRef Medline

Jeon D, Yang YM, Jeong MJ, Philipson KD, Rhim Hyewhon, Shin HS (2003) Enhanced learning and memory in mice lacking Na^+/Ca^{2+} exchanger 2. Neuron 38:965–976. CrossRef Medline

Jonas EA, Knox RJ, Smith TC, Wayne NL, Connor JA, Kaczmarek LK (1997) Regulation by insulin of a unique neuronal Ca^{2+} pool and neuropeptide secretion. Nature 385:343–346. CrossRef Medline

Juhaszova M, Shimizu H, Borin ML, Yip RK, Santiago EM, Lindenmayer GE, Blaustein MP (1996) Localization of the Na^+/Ca^{2+} exchanger in vascular smooth muscle, and in neurons and astrocytes. Ann N Y Acad Sci 779:318–335. CrossRef Medline

Juhaszova M, Church P, Blaustein MP, Stanley EF (2000) Location of calcium transporters at presynaptic terminals. Eur J Neurosci 12:839–846. CrossRef Medline

Kachoei BA, Knox RJ, Uthuza D, Levy S, Kaczmarek LK, Magoski NS (2006) A store-operated Ca^{2+} influx pathway in the bag cell neurons of *Aplysia.* J Neurophysiol 96:2688–2698. CrossRef Medline

Kaczmarek LK, Strumwasser F (1984) A voltage-clamp analysis of currents in isolated peptidergic neurons of *Aplysia.* J Neurophysiol 52:340–349. Medline

Kaczmarek LK, Jennings KR, Strumwasser F (1982) An early sodium and a late calcium phase in the afterdischarge of peptide-secreting neurons of *Aplysia.* Brain Res 238:105–115. CrossRef Medline

Kaftan EJ, Xu T, Abercrombie RF, Hille B (2000) Mitochondria shape hormonally induced cytoplasmic calcium oscillations and modulate exocytosis. J Biol Chem 18:25465–25470. CrossRef Medline

Karadjov JS, Kudzina LYu, Zinchenko VP (1986) TPP^+ inhibits Na^+ stimulated Ca^{2+} efflux from brain mitochondria. Cell Calcium 7:115–119. CrossRef Medline

Kawakami M, Uemura T, Hayashi R (1982) Electrophysiological correlates of pulsatile gonadotropin release in rats. Neuroendocrinology 55:63–67. Medline

Kim MH, Lee SH, Park KH, Ho WK, Lee SH (2003) Distribution of K^+-dependent Na^+/Ca^{2+} exchangers in the rat supraoptic magnocellular neuron is polarized to axon terminals. J Neurosci 23:11673–11680. Medline

Kim MH, Korogod N, Schneggenburger R, Ho WK, Lee SH (2005) Interplay between Na^+/Ca^{2+} exchangers and mitochondria in Ca^{2+} clearance at the calyx of held. J Neurosci 25:6057–6065. CrossRef Medline

Kim MS, Usachev YM (2009) Mitochondrial Ca^{2+} cycling facilitates activation of the transcription factor NFAT in sensory neurons. J Neurosci 29:12101–12114. CrossRef Medline

Knox RJ, Jonas EA, Kao LS, Smith PJ, Connor JA, Kaczmarek LK (1996) Ca^{2+} influx and activation of a cation current are coupled to intracellular Ca^{2+} release in peptidergic neurons of *Aplysia californica.* J Physiol 494:627–639. Medline

Krizaj D, Copenhagen DR (1998) Compartmentalization of calcium extrusion mechanisms in the outer and inner segments of photoreceptors. Neuron 21:249–256. CrossRef Medline

Kupfermann I, Kandel ER (1970) Electrophysiological properties and functional interconnections of two symmetrical neurosecretory clusters (bag cells) in abdominal ganglion of *Aplysia.* J Neurophysiol 33:865–876. Medline

Lee D, Lee KH, Ho WK, Lee SH (2007) Target cell-specific involvement of presynaptic mitochondria in post-tetanic potentiation at hippocampal mossy fiber synapses. J Neurosci 27:13603–13613. CrossRef Medline

Lincoln DW, Wakerley JB (1974) Electrophysiological evidence for the activation of supraoptic neurones during the release of oxytocin. J Physiol 242:533–554. Medline

Loechner KJ, Azhderian EM, Dreyer R, Kaczmarek LK (1990) Progressive potentiation of peptide release during a neuronal discharge. J Neurophysiol 63:738–744. Medline

Lupinsky DA, Magoski NS (2006) Ca^{2+}-dependent regulation of a non-selective cation channel from *Aplysia* bag cell neurones. J Physiol 575:491–506. CrossRef Medline

Magoski NS, Knox RJ, Kaczmarek LK (2000) Activation of a Ca^{2+}-permeable cation channel produces a prolonged attenuation of intracellular Ca^{2+} release in *Aplysia* bag cell neurones. J Physiol 522:271–283. CrossRef Medline

McDonough SI, Cseresnyes Z, Schneider MF (2000) Origin sites of calcium release and calcium oscillations in frog sympathetic neurons J Neurosci 20:9059–9070.

Michel S, Wayne NL (2002) Neurohormone secretion persists after post-afterdischarge membrane depolarization and cytosolic calcium elevation in peptidergic neurons in intact nervous tissue. J Neurosci 22:9063–9069. Medline

Morgans CW, El Far O, Berntson A, Wässle H, Taylor WR (1998) Calcium extrusion from mammalian photoreceptor terminals. J Neurosci 18: 2467–2474. Medline

Murthy VN, Sejnowski TJ, Stevens CF (2000) Dynamics of dendritic calcium transients evoked by quantal release at excitatory hippocampal synapses. Proc Natl Acad Sci U S A 97:901–906. CrossRef Medline

Naghdi S, Waldeck-Weiermair M, Fertschai I, Poteser M, Graier WF, Malli R (2010) Mitochondrial Ca^{2+} uptake and not mitochondrial motility is required for STIM1-Orai1-dependent store-operated Ca^{2+} entry. J Cell Sci 123:2553–2564. CrossRef Medline

Nakatani K, Chen C, Koutalos Y (2002) Calcium diffusion coefficient in rod photoreceptor outer segments. Biophys J 82:728–739. CrossRef Medline

Naraghi M (1997) T-jump study of calcium binding kinetics of calcium chelators. Cell Calcium 22:255–268. CrossRef Medline

Neering IR, McBurney RN (1984) Role for microsomal Ca^{2+} storage in mammalian neurones? Nature 309:158–160. CrossRef Medline

Neher E, Augustine GJ (1992) Calcium gradients and buffers in bovine chromaffin cells. J Physiol 450:273–301. Medline

Nowycky MC, Pinter MJ (1993) Time courses of calcium and calcium-bound buffers following calcium influx in a model cell. Biophys J 64:77–91. CrossRef Medline

Parekh AB, Putney JW Jr (2005) Store-operated calcium channels. Physiol Rev 85:757–810. CrossRef Medline

Pinsker HM, Dudek FE (1977) Bag cell control of egg-laying in freely behaving *Aplysia*. Science 197:490–493. CrossRef Medline

Putney JW Jr (2003) Capacitative calcium entry in the nervous system. Cell Calcium 34:339–344. CrossRef Medline

Rizzuto R, Pozzan T (2006) Microdomains of intracellular Ca^{2+}: molecular determinants and functional consequences. Physiol Rev 86:369–408. CrossRef Medline

Rizzuto R, Pinton P, Carrington W, Fay FS, Fogarty KE, Lifshitz LM, Tuft RA, Pozzan T (1998) Close contacts with the endoplasmic reticulum as determinants of mitochondrial Ca^{2+} responses. Science 280:1763–1766. CrossRef Medline

Sanchez-Armass S, Blaustein MP (1987) Role of sodium-calcium exchange in regulation of intracellular calcium in nerve terminals. Am J Physiol 252:595–603. Medline

Seidler NW, Jona I, Vegh M, Martonosi A (1989) Cyclopiazonic acid is a specific inhibitor of the Ca^{2+}-ATPase of sarcoplasmic reticulum. J Biol Chem 264:17816–17823. Medline

Shmigol A, Eisner DA, Wray S (1998) Carboxyeosin decreases the rate of decay of the $[Ca^{2+}]_i$ transient in uterine smooth muscle cells isolated from pregnant rats. Pflugers Arch 437:158–160. CrossRef Medline

Simons SB, Escobedo Y, Yasuda R, Dudek SM (2009) Regional differences in hippocampal calcium handling provide a cellular mechanism for limiting plasticity. Proc Natl Acad Sci U S A 106:14080–14084. CrossRef Medline

Smith SJ, MacDermott AB, Weight FF (1983) Detection of intracellular Ca^{2+} transients in sympathetic neurones using arsenazo III. Nature 304: 350–352. CrossRef Medline

Szebenyi SA, Laskowski AI, Medler KF (2010) Sodium/calcium exchangers selectively regulate calcium signaling in mouse taste receptor cells. J Neurophysiol 104:529–538. CrossRef Medline

Tam AK, Geiger JE, Hung AY, Groten CJ, Magoski NS (2009) Persistent Ca^{2+} current contributes to a prolonged depolarization in *Aplysia* bag-cell neurons. J Neurophysiol 102:3753–3765. CrossRef Medline

Tam AK, Gardam KE, Lamb S, Kachoei BA, Magoski NS (2011) Role for protein kinase C in controlling *Aplysia* bag cell neuron excitability. Neuroscience 179:41–55. CrossRef Medline

Tang Y, Zucker RS (1997) Mitochondrial involvement in post-tetanic potentiation of synaptic transmission. Neuron 18:483–491. CrossRef Medline

Thayer SA, Miller RJ (1990) Regulation of the intracellular free calcium concentration in single dorsal root ganglion neurones in vitro. J Physiol 425:85–115. Medline

Tidow H, Poulsen LR, Andreeva A, Knudsen M, Hein KL, Wiuf C, Palmgren MG, Nissen P (2012) A bimodular mechanism of calcium control in eukaryotes. Nature 491:468–472. CrossRef Medline

Vorndran C, Minta A, Poenie M (1995) New fluorescent calcium indicators designed for cytosolic retention or measuring calcium near membranes. J Biophys 69:2112–2124. CrossRef Medline

Wayne NL, Kim J, Lee E (1998) Prolonged hormone secretion from neuroendocrine cells of *Aplysia* is independent of extracellular Ca^{2+}. J Neuroendocrinol 10:529–537. CrossRef Medline

Wayne NL, Lee W, Michel S, De Quintana SB (2004) Post-afterdischarge depolarization does not stimulate prolonged neurohormone secretion but is required for activity-dependent stimulation of neurohormone biosynthesis from peptidergic neurons. Endocrinology 145:1678–1684. CrossRef Medline

Weiss S, Kohn E, Dadon D, Katz B, Peters M, Lebendiker M, Kosloff M, Colley NJ, Minke B (2012) Compartmentalization and Ca^{2+} buffering are essential for prevention of light-induced retinal degeneration. J Neurosci 32:14696–14708. CrossRef Medline

Werth JL, Thayer SA (1994) Mitochondria buffer physiological calcium loads in cultured rat dorsal root ganglion neurons. J Neurosci 14:348–356. Medline

Wheeler DG, Groth RD, Ma H, Barrett CF, Owen SF, Safa P, Tsien RW (2012) Cav1 and Cav2 channels engage distinct modes of Ca^{2+} signaling to control CREB-dependent gene expression. Cell 149:1112–1124. CrossRef Medline

Whim MD, Kaczmarek LK (1998) Expression of Kv3.1 in bag cell neurons prevents the induction of a depolarizing afterpotential. J Neurosci 18: 9171–9180. Medline

White BH, Kaczmarek LK (1997) Identification of a vesicular pool of calcium channels in the bag cell neurons of *Aplysia californica.* J Neurosci 17:1582–1595. Medline

White RJ, Reynolds IJ (1995) Mitochondria and Na/Ca exchange buffer glutamate-induced calcium loads in cultured cortical neurons. J Neurosci 15:1318–1328. Medline

Wilson GF, Richardson FC, Fisher TE, Olivera BM, Kaczmarek LK (1996) Identification and characterization of a Ca^{2+}-sensitive nonspecific cation channel underlying prolonged repetitive firing in *Aplysia* neurons. J Neurosci 16:3661–3671. Medline

Zenisek D, Matthews G (2000) The role of mitochondria in presynaptic calcium handling at a ribbon synapse. Neuron 25:229–237. CrossRef Medline

Zhang S, Yuan JX, Barrett KE, Dong H (2004) Role of Na^+/Ca^{2+} exchange in regulating cytosolic Ca^{2+} in cultured human pulmonary artery smooth muscle cells. Am J Physiol Cell Physiol 288:245–252. CrossRef Medline